Spring 2016

Elucidating the nanoscale structure of ionic liquids via molecular dynamics simulations

Jeevapani Jayaranga Hettige
University of Iowa

ELUCIDATING THE NANOSCALE STRUCTURE OF IONIC LIQUIDS VIA MOLECULAR DYNAMICS SIMULATIONS.

by

Jeevapani Jayaranga Hettige

A thesis submitted in partial fulfillment of the
requirements for the Doctor of Philosophy
degree in Chemistry
in the Graduate College of
The University of Iowa

May 2016

Thesis Supervisor: Professor Claudio J. Margulis

Graduate College
The University of Iowa
Iowa City, Iowa

CERTIFICATE OF APPROVAL

PH.D. THESIS

This is to certify that the Ph.D. thesis of

Jeevapani Jayaranga Hettige

has been approved by the Examining Committee for the thesis requirement for the Doctor of Philosophy degree in Chemistry at the May 2016 graduation.

Thesis committee: _____
Claudio Margulis, Thesis Supervisor

_____
Johna Leddy

_____
Sarah C. Larsen

_____
Alexei V. Tivanski

_____
Michael J. Schnieders

To my beloved family for their unconditional love

ACKNOWLEDGEMENTS

First and foremost, I would like to express my profound respect and deepest gratitude to my research supervisor, Prof. Claudio J. Margulis for the guidance, support and advice provided throughout my graduate life. Without his ongoing support, this dissertation would not have been a success. It was a great pleasure to work with Prof. Margulis for five years.

Also, I would like to express my gratitude to Prof. Edward Castner, Jr., our research collaborator at Rutgers, The State University of New Jersey for his excellent guidance and immense interest in my research, and the Castner group for carrying out X-ray scattering experiments that provided the experimental comparison for many of the systems we studied.

I would also like to thank Dr. Dale Swenson for teaching me the concepts of X-ray crystallography and for the instructive discussions. Without his help, understanding the advanced concepts of crystallography would have been a challenge to me.

In addition, I owe a deep sense of gratitude to the members of my academic committee for their time, guidance, valuable advise and instructive comments given about my research work. I also appreciate their effort in reading my dissertation and providing comments and suggestions.

I am thankful to the current and former members of Margulis group namely Sai (Dr. Ramadugu), Harsha (Dr. Annapureddy), Pablo (Dr. De Biase), Ying-Hua

(Dr. Chung), Ryan, Zhen, Alek, Fang, Chuck, Sharad (Dr. Yadav), Changhui (Dr. Xu), Mary, Hyunok, Kamal (Dr. Dhungana), Fei and Amith for making my graduate life easier and much fun. A special thank to Prof. Hemant K. Kashyap and soon to be Prof. Juan Carlos Araque for the enormous help given regarding my research work. Working in Margulis lab with my colleagues for five years, was a remarkable and wonderful experience to me.

I am extremely thankful to Ms. Brenna Faler, Mr. J.J. Urich, Mr. Bradley Carson, Mr. David Sansbury, Mr. Jon Yates and other systems administrators/ IT support consultants for handling our computer clusters effectively and assisting with issues related to hardware and software. Without their help, working on computational research would have been much more difficult.

Finally, my graduate life would not have been a success without the support from my family. The key to my success is the love, encouragement, support and advice I get from all my family members including my mom and my husband. I am extensively thankful to all family members for being my strength and courage throughout my life. I would also like to thank my Iowa Sri Lankan family for being there for me and creating a stress free environment so that I could work effectively.

ABSTRACT

In this dissertation, we present several structural studies carried out on novel materials commonly described as room-temperature ionic liquids. In many of these studies cations are bulky and amphiphilic and it can be said that they govern the liquid structural landscape. Many of the anions studied are less structurally rich, however their role in terms of X-ray experiments turns out to be fundamentally important. We will show that whereas cations may define structure, it is often the case that anions report on it. The main tools for the research described in this thesis are molecular dynamics and different aspects of theory of liquids. Much of the structural analysis presented here will be based on the X-ray structure function S(q) for which we propose additive partitions to better interpret features in the liquid phase.

As an example, dissection of the total structure functions into partial subcomponents functions such as polar-apolar and cation head- anion reveal alternations in the liquid phase unique to ionic liquids. A key concept associated with such alternations to be developed and described in thorough detail in this thesis is that of "peaks" and "antipeaks". The enhancement of similar-type group densities at a particular wave number, gives rise to peaks in the structure function whereas the depletion of different type group densities gives rise to 'antipeaks'. Hence, X-ray peaks and anti peaks reveal periodic order on different length scales in ionic liquid.

In cases, ionic liquids display what is called an X-ray first sharp diffraction peak. This is commonly the signature of polar-apolar alternation. The temperature

dependence of this structural peak can in some case be quite intriguing. One would expect that intermediate range order would diminish at higher temperatures but we have found that in the case of the popular tetradecyltrihexylphosphonium cation this trend is commonly reversed. This thesis proposes an explanation to this *a-priori* unexpected behavior.

Fluoroprotic ionic liquids that form hydrogen bonds and could potentially segregate into polar, apolar and fluoro dominated components have drawn a great deal of attention. We explore one such system in comparison to a non-fluorinated analog and discuss similarities and differences. Interestingly, the arrangement of alkyl and fluorinated tails in the system studied is defined by mandatory charge alternation which imposes alkyl fluorinated alternation as well with signatures in the structure function. The system studied also display a fully percolating charge network separated by decorating alkyl and fluoroprotic tails rendering the liquid bicontinuous.

PUBLIC ABSTRACT

In this dissertation we present several structural studies carried out on ionic liquids using tools derived from theory of liquids and molecular dynamics simulations. The study reveals structural information on liquids based on the ammonium, phosphonium and pyrrolidinium cations as well as on so-called triphillic ionic liquids. Even though the cations in ionic liquids govern the mesoscopic structure, in terms of X-ray experiments, anions frequently act as the *de facto* reporters of the structure. The anomalous temperature dependent behavior of the prepeak or first sharp diffraction peak in certain phosphonium based ionic liquids is a consequence of the enhancement in correlations between polar groups with increasing temperature. Our studies repeatedly reveal the role of what we have termed as peaks and antipeaks in association with liquid phase alternations. For example, a study highlighting peaks and antipeaks reveals that in the case of butylammonium pentadecafluoro-octanoate and butylammonium octanoate, the typical distance between adjacent charge alternating filaments that comprise a continuous network defines the first sharp diffraction peak.

TABLE OF CONTENTS

LIST OF TABLES

Table

LIST OF FIGURES

Figure

CHAPTER 1
INTRODUCTION

1.1 Introduction to Ionic Liquids.

Ionic liquids (ILs) are low melting salts, comprised entirely of cations and anions. The salts that melt below 100 ^{o}C, and often below room temperature are specifically known as room temperature ionic liquids (RTILs). A low melting salt, namely ethylammonium nitrate $C_2NH_8NO_3$ was first synthesized by Paul Walden who reported the physical properties of $C_2NH_8NO_3$(e.g. m.p. $\sim 12^{o}$C) in 1914. In here, the IL was synthesized by the neutralization of ethylamine with concentrated nitric acid. [10]

Some of the common ILs are composed of nitrogen or phosphorous containing heterocyclic (such as imidazolium or pyridinium)/ alkyl substituted cations, accompanied by inorganic anions such as $[BF_4^-]$, $[Cl^-]$, $[PF_6^-]$,or $[NO_3^-]$. Figure 1.1 shows some structures of cations and anions commonly used in ionic liquids.

Since ILs consist of two components (cation and anion) that can be varied, these solvents can be designed with a particular end use in mind. In other words, ILs give the opportunity to tune their specific properties for a particular application. Hence, the term 'designer solvents' [11, 12] has come into common practice. The fine

---

*A portion of this chapter is reproduced from Chemical Communications. vol. 48, page 5103, year 2012 by H. K. Kashyap, J. J. Hettige, H. V. R. Annapureddy and C. J. Margulis. DOI: 10.1039/C2CC30609C , The Journal of Physical Chemistry B. vol. 118, page 12706-12716, year 2014 by J.J. Hettige, J.C. Araque, and C.J. Margulis. Copyright - Appendix A.1 DOI: 10.1021/jp5068457, and The Journal of Physical Chemistry B. vol. 119 page 12727-12740, year 2015 by J. C. Araque, J. J. Hettige, and C. J. Margulis. Copyright - Appendix A.2 10.1021/acs.jpcb.5b05506

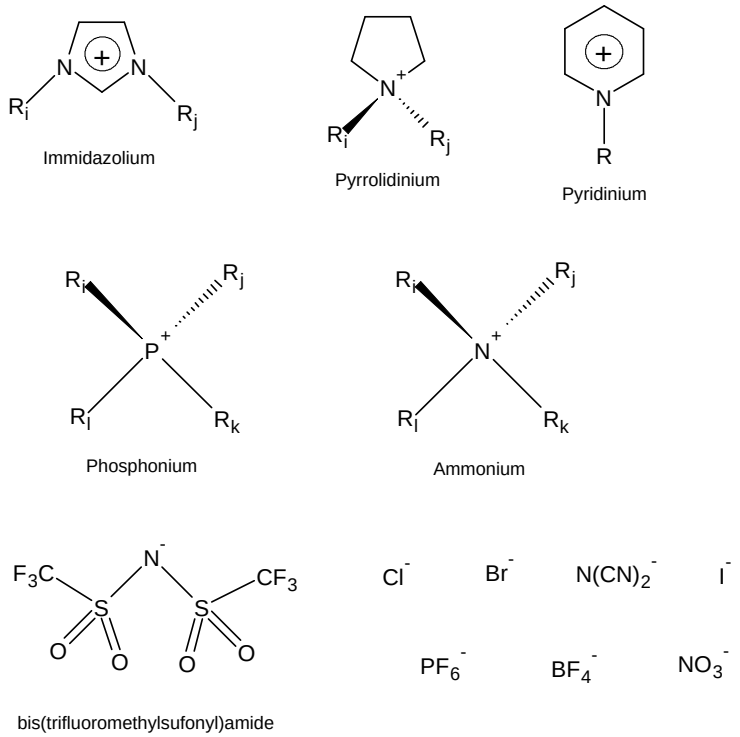

Figure 1.1: Chemical structures of some common ionic liquid cations and anions.

tuning of properties is possible by the variation of the chain length and branching of the alkyl groups incorporated into the cation or by changing the nature of the anion.[13] Properties such as melting point, viscosity, density, and hydrophobicity of an IL can easily be altered by incorporating simple changes to the structure of the constituent ions. [11, 12]

Owing to the fact that most ILs possess unique, versatile properties such as lower volatility,[14] higher thermal stability,[15] lower flammability,[16] and good conductivity,[17] they have drawn significant attention from many fields such as medicine, chemistry, physics and engineering.

It has been proposed that the physical properties that give access to a vast number of possible applications are likely associated with their nanoscale structure[18, 19, 20, 21]. Since this nanoscale structure[22] plays a major role in governing physical properties it is important to derive a clear atomistic picture to accompany X-ray and neutron scattering structural measurements. ILs are being used as the electrolyte in different electrochemical devices. One of the major issues related to the conventional batteries such as Li-ion batteries, is associated with safety.[23, 24] Unfavorable reactions occurring between the organic electrolytes present in these batteries could lead to an increase in the local heat and finally fire or explosion. Therefore necessary measures should always be taken in order to avoid such safety related issues. [25, 26] The use of less flammable and less volatile ILs in the place of flammable and volatile organic solutions reduces the risk of such thermal runaway. Because device safety can be increased by taking advantage of physical properties such as nonvolatility and non-

flammability, ILs are also considered as liquid electrolytes in electrochemical energy storage devices such as double layer capacitors.[27, 28]

Certain ILs have also proved to be advantageous for organic reactions. Increased rates and control of product distribution, ease of product recovery, ease of recycling and catalyst immobilization have been reported in the literature.[29, 30] Moreover, it has been claimed that ILs can be used to prevent much of the need for controlling toxic emissions and/or combustion risks associated with the use of volatile organic compounds (VOCs). Currently, ILs are used in organic reactions such as neucleophilic aromatic substitution, Heck reaction, Diels Alder reaction, BaylisHillman reaction and in the formation of N-heterocyclic carbenes.[30] In addition, ILs are being used to replace organic solvents in biochemical reactions.[31, 32, 33, 34] They are applied to various biochemical processes such as enzymatic polymerization in ILs, protein and enzyme extraction for biocatalysis and the production of biofuels.

Many of the techniques currently used in cellulose processing are considered to be nongreen. The term 'green solvents' refers to those that cause benign environmental effects, and most ILs have been termed 'green solvents' due to their negligible vapor pressure and nonflammable properties. Certain 'green' ILs are being used as nonderivatizing solvents for cellulose processing.

Solvent extraction has been very well known as an effective technique for the separation of metal ions such as Hg^{2+}, Cd^{2+}, Cu^{2+}, Ag^{+}, and Pb^{2+} on a large industrial scale. [35, 36] However, the conventional solvents used in metal ion extraction are flammable and volatile. ILs have the ability to replace traditional VOCs

in liquid/liquid extraction of metal ions. They also exhibit several other convenient properties such as good thermal stability and the ability to solubilize a wide range of solutes which makes them appealing for industrial applications. ILs incorporated with specific chelating groups in order to address a specific function, are known as Task Specific Ionic Liquids (TSILs). TSILs have been recently proposed as a new approach for metal ion extraction.[37] In particular, ILs show a higher efficiency in mercury extraction.

In the case of industrial CO_2 extraction, ILs have been used as solvent reagents for separating CO_2 from other gases.[38] In addition, it is well known that many popular drugs are sparingly soluble and almost hardly enter a formulation stage due to poor solubility and difficulties in delivery.[39] There is a clear need for the development of newer drug delivery methods that can reduce toxicity and facilitate administration. ILs are being pursued as means to enhance solubility of sparingly soluble/insoluble drugs. [40, 39].

1.2 Molecular Dynamics Simulations.

The work described in this thesis is mostly computational in nature. The structure of ILs is studied using the Molecular Dynamics (MD) simulation technique as well as other mathematical tools. The MD algorithmic aspects have been thoroughly described in many other documents and need not be repeated here.[41, 42, 43, 44, 45, 46] However, specific details will be highlighted throughout this thesis when needed.

The functional form and parameter sets used to calculate the potential energy

of a system of particles is known as the 'force field'. In our study, classical MD simulations were performed using the GROMACS software package[42] and a potential energy function of the form,

$$U = U_{stretch} + U_{bend} + U_{torsion} + U_{LJ} + U_{coulomb} \tag{1.1}$$

where,

$$U_{stretch} = \sum_{bonds} K_r(r - r_{eq})^2 \tag{1.2}$$

$$U_{bend} = \sum_{angles} K_\theta(\theta - \theta_{eq})^2 \tag{1.3}$$

$$U_{torsion} = \sum_{dihedrals} \sum_{n=o}^{5} C_n(cos(\phi))^n \tag{1.4}$$

$$U_{LJ} = \sum_{i<j} 4\epsilon_{ij}[(\frac{\sigma_{ij}}{r_{ij}})^{12} - (\frac{\sigma_{ij}}{r_{ij}})^6] \tag{1.5}$$

$$U_{coulomb} = \sum_{i<j} \frac{q_i q_j}{r_{ij}} \tag{1.6}$$

Where $U_{stretch}$ accounts for the interaction between pairs of bonded atoms. The potential energy component is modelled by a harmonic potential that results in an increase in energy as the bond length r deviates from the reference (equilibrium) value, r_{eq}. The potential energy term U_{bend} is modelled using a harmonic potential. The third term of eq. 1.1, is used to model the torsional energy changes of molecules with bond rotation. The first three terms are considered to be bonded interactions

while, the fourth and fifth terms are considered non-bonded interactions. For the force fields we have used which are referenced later in specific sections of this thesis, this type of non-bonded interactions are calculated between pairs of atoms either in different molecules or in the same molecule, but at least three bonds away (1-4 pairs); this is the typical OPLS convention.[47, 48, 49] U_{LJ} stands for the Lennard-Jones potential which results due to van der Waals interactions while $U_{coulomb}$ stands for the Coulomb potential term which is a consequence of electrostatic interactions. [42, 46] All our studies use periodic boundary conditions and the minimum image convention.[41]

1.3 Structure Function.

The structure function (S(q)) is the fundamental mathematical connection between microscopic pair distribution functions and the experimentally observed X-ray scattering intensity. In our studies, S(q) is computed using the following equation;

$$S(q) = \frac{\rho_o \sum_i \sum_j x_i\, x_j\, f_i(q) f_j(q) \int_0^{L/2} 4\pi r^2 (g_{ij}(r) - 1) \frac{\sin qr}{qr} W(r) dr}{\left[\sum_i x_i f_i(q)\right]^2} \tag{1.7}$$

where, $g_{ij}(r)$ stands for the full system radial distribution function(RDF) comprising both intra- and inter-molecular pair of atomic species of type i and j, and the RDF is associated with the probability to find an atom in a shell r at a distance r of another atom chosen as a reference point at the origin; x_i and x_j are the corresponding atomic

mol fractions of atoms of type i and j and $f_i(q)$, $f_j(q)$ are tabulated X-ray atomic form factors that can be found in reference [50]. In eq. 1.7 the total number density for the system is denoted as ρ_o and the box length for our periodically replicated system is referred as L. As is common practice, a Lorch Window Function[51, 52] is used to reduce the effect of finite truncation of $g_{ij}(r)$ at large values of r.

$$W(r) = \sin(2\pi r/L)/(2\pi r/L) \tag{1.8}$$

The scattering vector, q is given by eq. 1.9

$$q = \frac{4\pi \sin\theta}{\lambda} \tag{1.9}$$

Where, 2θ is the angle between the incident X-ray beam and the detector, and λ is the wavelength of X-ray.

Figure 1.2 shows the total S(q)s obtained for a series of liquids including pyrrolidinium, phosphonium, ammonium, and imidazolium cations. Mainly, three peaks can be identified in the total S(q) of most of these ILs. In several recent publications we have described the peak that appears at a larger q ($\sim 1.5\mathring{A}^{-1}$) as the adjacency peak; the origin of this peak is due to nonperiodic correlations between adjacent atoms. These correlations can be both intramolecular and intermolecular in nature. A feature often appearing in the q range ($\sim 0.75\mathring{A}^{-1}$) can be ascribed to charge alternation. Finally, the peak that appears at the smallest q range ($\sim 0.5\mathring{A}^{-1}$), namely the prepeak or first sharp diffraction peak (FSDP) is a consequence of the alternation between polar and apolar groups (polarity alternation). Videlicet, the prepeak indicates the largest length scales present in the system. Intriguingly,

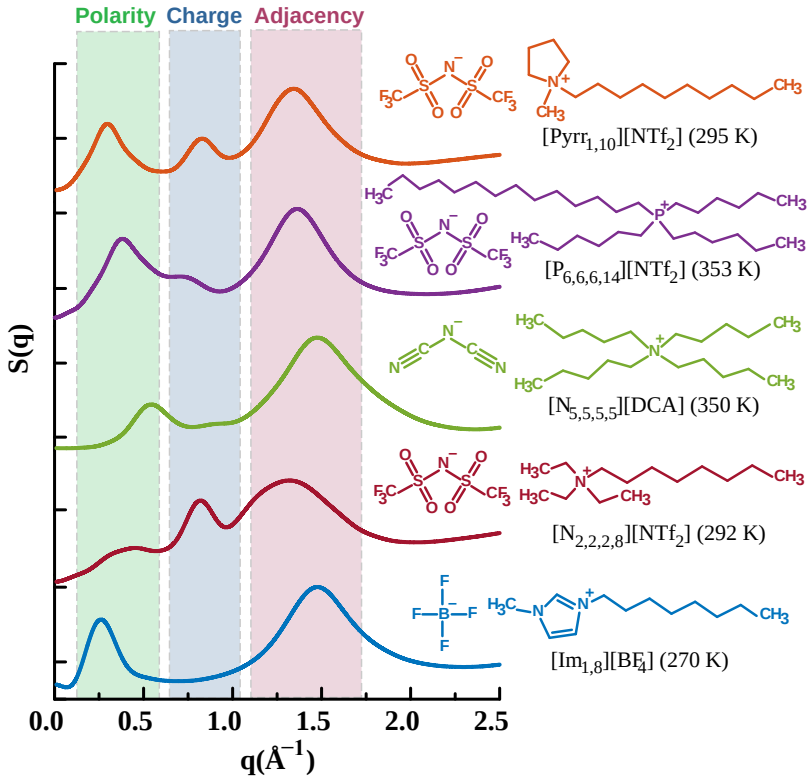

Figure 1.2: Computationally derived S(q) for 1-decyl-1-methylpyrrolidinium bis (trifluoromethylsulfonyl)amide, tetradecyltrihexylphosphonium bis (trifluoromethylsulfonyl)amide, tetrapentylammonium dicyanamide, triethyloctylammonium bis (trifluoromethylsulfonyl)amide and 1-octyl-3-methylimidazolium tetrafluoroborate ionic liquids.

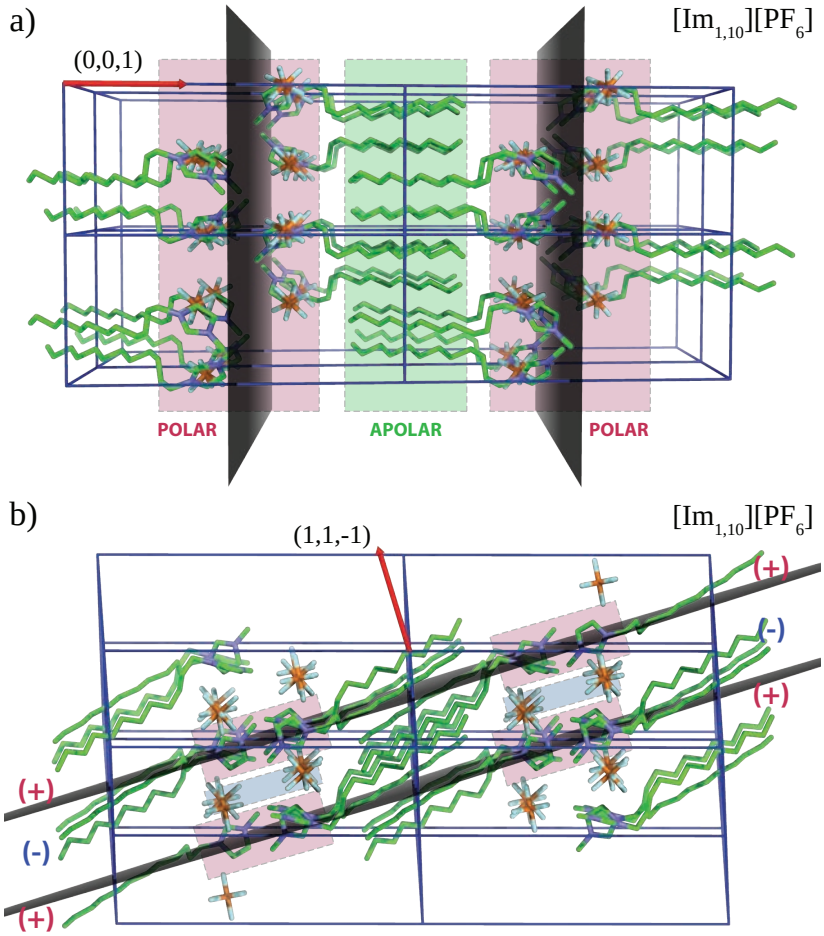

Figure 1.3: Crystal structure of $[Im_{10,1}][PF_6]$ showing (a) polarity alternation across Miller plane (0,0,1) and (b) charge alternation across Miller plane (1,1,-1). These two symmetries, charge and polarity alternation, that are present in the crystalline state persist in the liquid phase and become the defining features of ionic liquid morphology. See ref [1]

both charge and polarity alternation features are conserved in the corresponding crystal structure. (See Fig. 1.3 for a pictorial representation of polarity and charge alternations.) However, it is noticeable that some ILs are missing some peaks in the total S(q): An illustration for the observation of missing peaks will be discussed in Chapter 3 in detail.

1.4 Partial Structure Functions.(Partial S(q))

Partitioning of S(q) into cationic, anionic and their cross correlations such that $S(q) = S^{c-c}(q) + S^{c-a}(q) + S^{a-c}(q) + S^{a-a}(q)$ leads to the following definitions of subcomponents:[53]

$$\begin{aligned} S^{c-c}(q) &= \frac{\rho_o \sum_i \sum_j x_i\, x_j f_i(q) f_j(q)}{\left[\sum_i x_i f_i(q)\right]^2} \int_0^\infty 4\pi r^2 \left[g_{ij}^{c-c}(r) - \lim_{r\to\infty} g_{ij}^{c-c}(r)\right] \frac{\sin(qr)}{qr} dr \\ S^{a-a}(q) &= \frac{\rho_o \sum_i \sum_j x_i\, x_j f_i(q) f_j(q)}{\left[\sum_i x_i f_i(q)\right]^2} \int_0^\infty 4\pi r^2 \left[g_{ij}^{a-a}(r) - \lim_{r\to\infty} g_{ij}^{a-a}(r)\right] \frac{\sin(qr)}{qr} dr \quad (1.10) \end{aligned}$$

and

$$S^{c-a}(q) + S^{a-c}(q) = \frac{\rho_o \sum_i \sum_j x_i\, x_j f_i(q) f_j(q)}{\left[\sum_i x_i f_i(q)\right]^2} \left\{ \begin{array}{l} \int_0^\infty 4\pi r^2 \left[g_{ij}^{c-a}(r) - \lim_{r\to\infty} g_{ij}^{c-a}(r)\right] \frac{\sin(qr)}{qr} dr \\ + \int_0^\infty 4\pi r^2 \left[g_{ij}^{a-c}(r) - \lim_{r\to\infty} g_{ij}^{a-c}(r)\right] \frac{\sin(qr)}{qr} dr \end{array} \right\} \quad (1.11)$$

Here, $g_{ij}^{c-a}(r)$ is the radial distribution function for the ith type of atom in the

cation and the jth type of atom in the anion and are given by,[53]

$$
\begin{aligned}
g_{ij}^{c-c}(r) &= \frac{V}{N_i N_j}\sum_i^{N_i^c}\sum_j^{N_j^c}\frac{\delta(r_{ij}-r)}{\frac{4}{3}\pi((r+dr)^3-r^3)},\\
g_{ij}^{c-a}(r) &= \frac{V}{N_i N_j}\sum_i^{N_i^c}\sum_j^{N_j^a}\frac{\delta(r_{ij}-r)}{\frac{4}{3}\pi((r+dr)^3-r^3)},\\
g_{ij}^{a-c}(r) &= \frac{V}{N_i N_j}\sum_i^{N_i^a}\sum_j^{N_j^c}\frac{\delta(r_{ij}-r)}{\frac{4}{3}\pi((r+dr)^3-r^3)},\\
g_{ij}^{a-a}(r) &= \frac{V}{N_i N_j}\sum_i^{N_i^a}\sum_j^{N_j^a}\frac{\delta(r_{ij}-r)}{\frac{4}{3}\pi((r+dr)^3-r^3)},
\end{aligned}
\tag{1.12}
$$

where V is the volume, N_i is the total number of atoms of type i in the system, and N_i^c, N_i^a are the number of atoms of type i in cations and anions, respectively.

One can further split the cation-cation partial structure function such that $S^{c-c}(q) = S^{c_{Head}-c_{Head}}(q) + S^{c_{Head}-c_{Tail}}(q) + S^{c_{Tail}-c_{Head}}(q) + S^{c_{Tail}-c_{Tail}}(q)$ as:

$$
\begin{aligned}
S^{c_{Head}-c_{Head}}(q) &= \frac{\rho_o \sum_i \sum_j x_i\, x_j f_i(q) f_j(q)}{\left[\sum_i x_i f_i(q)\right]^2}\int_0^\infty 4\pi r^2\left[g_{ij}^{c_{Head}-c_{Head}}(r) - \lim_{r\to\infty} g_{ij}^{c_{Head}-c_{Head}}(r)\right]\frac{\sin(qr)}{qr}dr\\
S^{c_{Tail}-c_{Tail}}(q) &= \frac{\rho_o \sum_i \sum_j x_i\, x_j f_i(q) f_j(q)}{\left[\sum_i x_i f_i(q)\right]^2}\int_0^\infty 4\pi r^2\left[g_{ij}^{c_{Tail}-c_{Tail}}(r) - \lim_{r\to\infty} g_{ij}^{c_{Tail}-c_{Tail}}(r)\right]\frac{\sin(qr)}{qr}dr
\end{aligned}
$$

and

$$
S^{c_{Head}-c_{Tail}}(q) + S^{c_{Tail}-c_{Head}}(q) =
$$

$$
\frac{\rho_o \sum_i \sum_j x_i\, x_j f_i(q) f_j(q)}{[\sum_i x_i f_i(q)]^2}\left\{\begin{array}{c}\displaystyle\int_0^\infty 4\pi r^2\left[g_{ij}^{c_{Head}-c_{Tail}}(r) - \lim_{r\to\infty} g_{ij}^{c_{Head}-c_{Tail}}(r)\right]\frac{\sin(qr)}{qr}dr\\ \displaystyle+\int_0^\infty 4\pi r^2\left[g_{ij}^{c_{Tail}-c_{Head}}(r) - \lim_{r\to\infty} g_{ij}^{c_{Tail}-c_{Head}}(r)\right]\frac{\sin(qr)}{qr}dr\end{array}\right\}
\tag{1.13}
$$

In eqns. 1.13 $g_{ij}^{c_{Head}-c_{Head}}(r)$, $g_{ij}^{c_{Tail}-c_{Tail}}(r)$, $g_{ij}^{c_{Head}-c_{Tail}}(r)$ and $g_{ij}^{c_{Tail}-c_{Head}}(r)$ are given by,

$$\begin{aligned}
g_{ij}^{c_{Head}-c_{Head}}(r) &= \frac{V}{N_i N_j} \sum_i^{N_i^{c_{Head}}} \sum_j^{N_j^{c_{Head}}} \frac{\delta(r_{ij}-r)}{\frac{4}{3}\pi((r+dr)^3-r^3)}, \\
g_{ij}^{c_{Tail}-c_{Tail}}(r) &= \frac{V}{N_i N_j} \sum_i^{N_i^{c_{Tail}}} \sum_j^{N_j^{c_{Tail}}} \frac{\delta(r_{ij}-r)}{\frac{4}{3}\pi((r+dr)^3-r^3)}, \\
g_{ij}^{c_{Head}-c_{Tail}}(r) &= \frac{V}{N_i N_j} \sum_i^{N_i^{c_{Head}}} \sum_j^{N_j^{c_{Tail}}} \frac{\delta(r_{ij}-r)}{\frac{4}{3}\pi((r+dr)^3-r^3)}, \\
g_{ij}^{c_{Tail}-c_{Head}}(r) &= \frac{V}{N_i N_j} \sum_i^{N_i^{c_{Tail}}} \sum_j^{N_j^{c_{Head}}} \frac{\delta(r_{ij}-r)}{\frac{4}{3}\pi((r+dr)^3-r^3)}. \qquad (1.14)
\end{aligned}$$

In eqns. 1.14, $N_i^{c_{Head}}$, $N_i^{c_{Tail}}$ are the total number of atoms of type i in the polar head and apolar tail of the cation respectively.

Similarly one can split the cation-anion partial structure function so that $[S^{c-a}(q) + S^{a-c}(q)] = S^{c_{Head}-a}(q) + S^{a-c_{Head}}(q) + S^{c_{Tail}-a}(q) + S^{a-c_{Tail}}(q)$ as:

$$\begin{aligned}
&S^{c_{Head}-a}(q) + S^{a-c_{Head}}(q) = \\
&\frac{\rho_o \sum_i \sum_j x_i\, x_j f_i(q) f_j(q)}{\left[\sum_i x_i f_i(q)\right]^2} \left\{ \begin{array}{l} \int_0^\infty 4\pi r^2 \left[g_{ij}^{c_{Head}-a}(r) - \lim_{r\to\infty} g_{ij}^{c_{Head}-a}(r) \right] \frac{\sin(qr)}{qr} dr \\ + \int_0^\infty 4\pi r^2 \left[g_{ij}^{a-c_{Head}}(r) - \lim_{r\to\infty} g_{ij}^{a-c_{Head}}(r) \right] \frac{\sin(qr)}{qr} dr \end{array} \right\} \\
&S^{c_{Tail}-a}(q) + S^{a-c_{Tail}}(q) = \\
&\frac{\rho_o \sum_i \sum_j x_i\, x_j f_i(q) f_j(q)}{\left[\sum_i x_i f_i(q)\right]^2} \left\{ \begin{array}{l} \int_0^\infty 4\pi r^2 \left[g_{ij}^{c_{Tail}-a}(r) - \lim_{r\to\infty} g_{ij}^{c_{Tail}-a}(r) \right] \frac{\sin(qr)}{qr} dr \\ + \int_0^\infty 4\pi r^2 \left[g_{ij}^{a-c_{Tail}}(r) - \lim_{r\to\infty} g_{ij}^{a-c_{Tail}}(r) \right] \frac{\sin(qr)}{qr} dr \end{array} \right\} \qquad (1.15)
\end{aligned}$$

Here, $g_{ij}^{c_{Head}-a}(r)$, $g_{ij}^{c_{Tail}-a}(r)$, $g_{ij}^{a-c_{Head}}(r)$ and $g_{ij}^{a-c_{Tail}}(r)$ are given by,

$$\begin{aligned}
g_{ij}^{c_{Head}-a}(r) &= \frac{V}{N_i N_j} \sum_i^{N_i^{c_{Head}}} \sum_j^{N_j^a} \frac{\delta(r_{ij}-r)}{\frac{4}{3}\pi((r+dr)^3-r^3)}, \\
g_{ij}^{c_{Tail}-a}(r) &= \frac{V}{N_i N_j} \sum_i^{N_i^{c_{Tail}}} \sum_j^{N_j^a} \frac{\delta(r_{ij}-r)}{\frac{4}{3}\pi((r+dr)^3-r^3)}, \\
g_{ij}^{a-c_{Head}}(r) &= \frac{V}{N_i N_j} \sum_i^{N_i^a} \sum_j^{N_j^{c_{Head}}} \frac{\delta(r_{ij}-r)}{\frac{4}{3}\pi((r+dr)^3-r^3)}, \\
g_{ij}^{a-c_{Tail}}(r) &= \frac{V}{N_i N_j} \sum_i^{N_i^a} \sum_j^{N_j^{c_{Tail}}} \frac{\delta(r_{ij}-r)}{\frac{4}{3}\pi((r+dr)^3-r^3)}.
\end{aligned} \tag{1.16}$$

Experimentally, the total S(q) is determined from the coherent X-ray scattering intensity, $I_{coh}(q)$, using eq. 1.17

$$S(q) = \frac{I_{coh}(q) - \sum_i x_i f_i^2(q)}{[\sum_i x_i f_i(q)]^2}. \tag{1.17}$$

1.5 Inverting $S(q)$ to Discover Important Real Space Liquid Structural Motifs.

The work discussed in section 1.3 and several previous articles[54, 55, 56] has enabled us to achieve an understanding of ILs in terms of three main features, namely charge alternation, polarity alternation and diverse adjacency correlations. Whereas this understanding has tremendously helped in properly analyzing $S(q)$, many ILs show the same three peaks. Going beyond this analysis to fully discern the 3 dimensional real space context in which such adjacencies and alternations manifest has not been easy.

We therefore seek to mathematically identify those characteristic atomic correlations that at distances around $2\pi/q$ contribute significantly to $S(q)$. The problem

with what has been our proverbial approach to computing partial contributions to $S(q)$[54, 56] is that identifying particular atomic contributions is difficult in real space by using equation 1.7. The difficulty arises because the information about individual atomic pairs is not directly available from $g(r)$ since this is a collective function. This information becomes readily available if instead of writing $S(q)$ as a 3D Fourier transform of $g(r)$ we instead cast it in terms of a sum of Fourier space static correlation functions as in Eq. 1.18.

$$S(q) = \frac{\sum_i \sum_j f_i(q) f_j(q) \left[\frac{1}{N}\langle \rho^i_{\mathbf{q}} \rho^j_{-\mathbf{q}} \rangle - x_i \delta_{i,j}\right]}{\left[\sum_i x_i f_i(q)\right]^2} \tag{1.18}$$

In eq. 1.18 the angle brackets denote the ensemble average of Fourier space densities defined in eq. 1.19,

$$\begin{aligned} \rho^i_{\mathbf{q}} &= \sum_{\alpha=1}^{N_i} \exp(-i\mathbf{q}\cdot\mathbf{r}_\alpha) \\ \rho^j_{-\mathbf{q}} &= \sum_{\beta=1}^{N_j} \exp(i\mathbf{q}\cdot\mathbf{r}_\beta), \end{aligned} \tag{1.19}$$

where N_i and N_j are the total number of atoms of species i and j respectively. Equation 1.18 can be easily derived by disregarding forward scattering and noticing that[57]

$$\frac{1}{N}\langle \rho^i_{\mathbf{q}} \rho^j_{-\mathbf{q}} \rangle = x_i \delta_{i,j} + \rho_o x_i x_j \int_0^{L/2} 4\pi r^2 (g_{ij}(r) - 1) \frac{\sin qr}{qr} dr. \tag{1.20}$$

During simulation the ensemble average $\langle \rho^i_{\mathbf{q}} \rho^j_{-\mathbf{q}} \rangle$ is obtained as a sum over exponentials $\rho^{i_\alpha}_{\mathbf{q}} \rho^{j_\beta}_{-\mathbf{q}} = \exp(-i\mathbf{q}\cdot(\mathbf{r}_\alpha - \mathbf{r}_\beta))$ that is real, where i_α and j_β correspond to atoms α and β from species i and j, respectively. It is clear now that one can identify for a q value of interest atomic pairs α and β that for each simulation frame significantly

contribute to $\langle \rho^i_{\mathbf{q}} \rho^j_{-\mathbf{q}} \rangle$. Many such important contributions exist at wave numbers corresponding to peaks and antipeaks in the partial subcomponents of $S(q)$. However, only a few structural motifs satisfy both that their contribution at the q value of interest is large and atomic distance is close to $d_{\alpha\beta} = 2\pi/q$. To easily identify those pairs of atoms that satisfy both requirements we propose to use the following function:

$$S^{w_{i,j}}_{\alpha\beta}(q) = \frac{1}{\left|\frac{2\pi}{q} - d_{\alpha\beta}\right|} Re(S^{i,j}_{\alpha\beta}(q)), \tag{1.21}$$

where in analogy with eq. 1.18, $S^{i,j}_{\alpha\beta}(q)$ is defined as

$$S^{i,j}_{\alpha\beta}(q) = \frac{f_i(q) f_j(q) \left[\frac{1}{N}\overline{\rho^{i_\alpha}_{\mathbf{q}} \rho^{j_\beta}_{-\mathbf{q}}} - x_i \delta_{i,j}\right]}{\left[\sum_i x_i f_i(q)\right]^2}. \tag{1.22}$$

The overbar in eq. 1.22 implies an angular average over $\mathbf{q}$ vectors of the same magnitude. Equation 1.21 identifies pairs of atomic contributions that significantly contribute to $S(q)$ and that at the same time are resonant with the Bragg condition at wave number q. Thus, equation 1.21 provides a tool to identify individual structural motifs in real space (relative distance and orientation) that at distances $2\pi/q$ give rise to the different peaks and antipeaks in partial subcomponents of $S(q)$.

1.6 Simulation Protocol.

In this section, a concise and general description of the computational and simulation protocol used in the structural studies related to this dissertation will be discussed. However, the computational and simulation information unique to each

study will be discussed in the corresponding chapter, along with the discussion of results.

For the studies discussed in this dissertation, all MD simulations were carried out using the GROMACS package[58, 59],(version 4.5.5) at the single-precision level. A simulation box of 1000 cation and anion ion pairs were used to model each IL system and ensure proper sampling. As a preliminary step, first each system was energy minimized using the steepest descent algorithm, with full atomic charges, to adjust the potential to their local minima. Second, each system was equilibrated for at least 2 ns by scaling the atomic charges and raising and lowering the temperature. Finally, each system was run in NPT ensemble (constant number of particles, constant pressure and temperature). Atomic coordinates of the last 2 ns of the trajectory were stored every 1 ps to calculate liquid structural properties. During production runs Nose-Hoover thermostat[60, 61] and Parrinello-Rahman[62] barostat were used to set the temperature and pressure, respectively. In all cases equations were integrated using the leap-frog algorithm. Simulations were run under periodic boundary conditions using the particle mesh Ewald algorithm[63, 64] with a grid spacing of 0.08 nm and interpolation order of 6. Radial cutoffs for the real space part of the Coulomb interaction and for the Lennard-Jones interactions were set to 1.5 nm. In each study, slight alterations were incorporated into the computational and simulation method discussed in this chapter, in order to fit the IL system studied and the objective of the study. The adjustments made to the above mentioned methodology in order to suit each study, will be discussed in the subsequent chapters.

CHAPTER 2
THE ASSOCIATION BETWEEN SAXS ANTI-PEAKS AND POLARITY AND CHARGE ALTERNATIONS IN ROOM TEMPERATURE IONIC LIQUIDS.

2.1 Introduction

In Chapter 1, the concept of adjacency, charge and polarity alternation were introduced. In the current chapter, we attempt to provide insightful discussion on the structure of certain pyrrolidinium based ILs, and their multiple length scale features based on the concept of same spatial periodicity peaks and anti-peaks. Structural patterns that have the same spatial periodicity but a phase offset give rise to peaks(positive-going) and anti-peaks(negative-going) at the same wave number (q value). The enhancements and depletions of the +/- or polar/apolar densities, highlighted by peaks and anti-peaks at the same q value, reveal the structural heterogeneity present in many of these ILs.

Because pyrrolidinium RTILs are promising media with wide electrochemical windows[65] suitable for applications in Li ion batteries,[66] we have chosen for this study 1-alkyl-1-methylpyrrolidinium bis(trifluoromethylsulfonyl)amide, $\mathrm{Pyrr}_{1,n}{}^{+}\mathrm{NTf}_2{}^{-}$, RTILs with $n = 4$, 6, 8 and 10 (see fig. 2.1) for which a full range of X-ray scattering data has recently been made available by the groups of Castner[2] and Cummings.[67] The work by the group of Cummings[67] also provides important simulation insight

*A portion of this chapter is reproduced from Chemical Communications. vol. 48, page 5103, year 2012 by H. K. Kashyap, J. J. Hettige, H. V. R. Annapureddy and C. J. Margulis. DOI: 10.1039/C2CC30609C

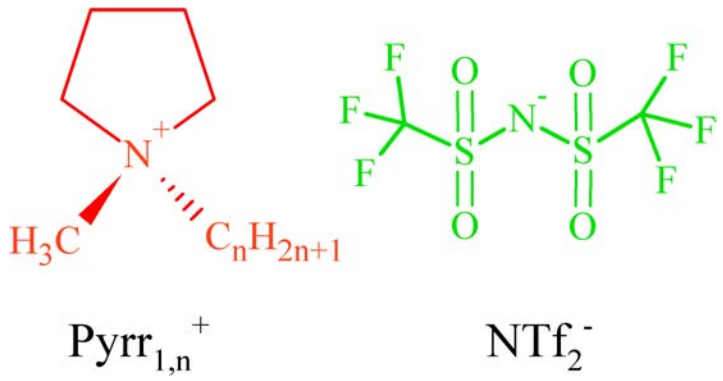

Figure 2.1: Chemical Structure of 1-alkyl-1-methylpyrrolidinium cation (left) and bis (triflouromethylsulfonyl)amide anion (right).

into the analysis of S(q).

In addition to the general methodology we use in preparing an IL for calculations, for the study discussed in this chapter, we used the Lopes and Padua[68] partial charges for cations and anions. Bonded and Lennard-Jones (LJ) energy parameters were taken from the OPLS-AA[47] force field as suggested by Lopes and Padua.[68] However, the torsional energy parameters for CT-CT-CT-CT, CT-CT-CT-HC and HC-CT-CT-HC dihedrals for alkyl carbons and hydrogens were taken from the improved OPLS-AA(2001) parameter set[48]. Each system was simulated in a simple cubic box consisting of 3000 ion pairs. Subsequently, each system was run in the NPT ensemble for at least 3.5 ns at 295 K and 1 bar. The final simulated bulk densities of $\mathrm{Pyrr}_{1,n}{}^{+}\mathrm{NTf}_2{}^{-}$ liquids for $n = 4$, 6, 8 and 10 were 1.46, 1.39, 1.33 and 1.29 gm/cc, respectively.

2.2 Results and Discussion

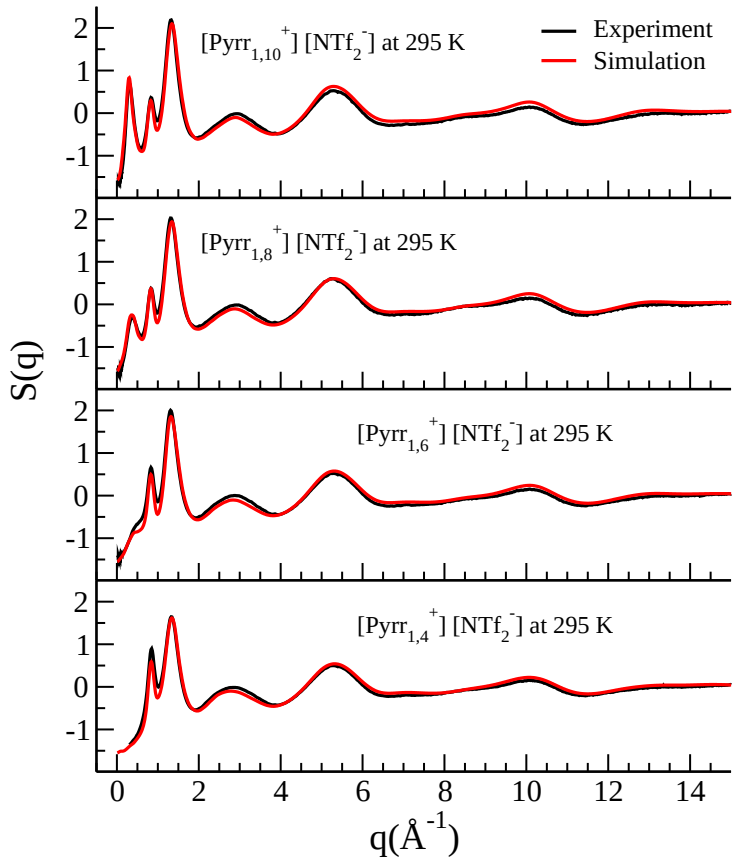

Figure 2.2: Comparison between experiments and simulations of the X-ray structure function S(q) for $Pyrr_{1,n}{}^{+}NTf_2{}^{-}$ at 295 K. Experimental data from the Castner group.[2]

Fig. 2.2 shows the good level of agreement with experiment that force fields[69, 47, 48] can achieve when combined with very large (3000 ion pairs) simulation volumes. Agreement with experiment is most perfect for longer chain liquids. Prior

simulations using a different force field and only 125 or 250 pairs produced a spurious prepeak in short alkyl tail systems.[67] This chapter basically focuses on the three characteristic peaks observed in S(q) at q < 2 Å^{-1} for $n = 8$ and 10. These peaks occur at around 0.35, 0.85 and 1.35 Å^{-1} respectively.[2, 67] $Pyrr_{1,6}{}^{+}NTf_2{}^{-}$ shows the onset of a prepeak but this feature is absent in the case of $Pyrr_{1,4}{}^{+}NTf_2{}^{-}$. Using the methodology proposed by Santos and coworkers,[53] Li *et al.*[67] partitioned S(q) into relevant subcomponents and arrived at the conclusion that long alkyl tail $Pyrr_{1,n}{}^{+}$ showed signs of hydrophobic aggregation. Herein, we attempt to provide a simple and unifying picture of the structure of many RTILs and their multiple length scale features based on the concept of same spatial periodicity peaks and anti-peaks. It is clear from extensive simulation literature[70, 71, 72, 73, 74, 75, 76, 77, 1, 67] that the relevant components are the charged groups and the hydrophobic groups. As it turns out charge alternation and polar-apolar alternation play a role on two different length scales.

Figure 2.3 shows total S(q) as well as cation-cation, anion-anion and cation-anion subcomponents.

Three key findings are derived from this figure:

(1) The peak at around q = 1.35 Å^{-1} has predominant contribution from cation-anion correlations (in fact, mostly cation polar head-anion correlations as can be seen in Fig. 2.4). Also in Fig. 2.3, the cation-cation subcomponent increases from a negligible contribution when $n = 4$ to a significant contribution when $n = 10$. This can be appreciated in Fig. 2.3 from the relative contribution of red and blue lines to

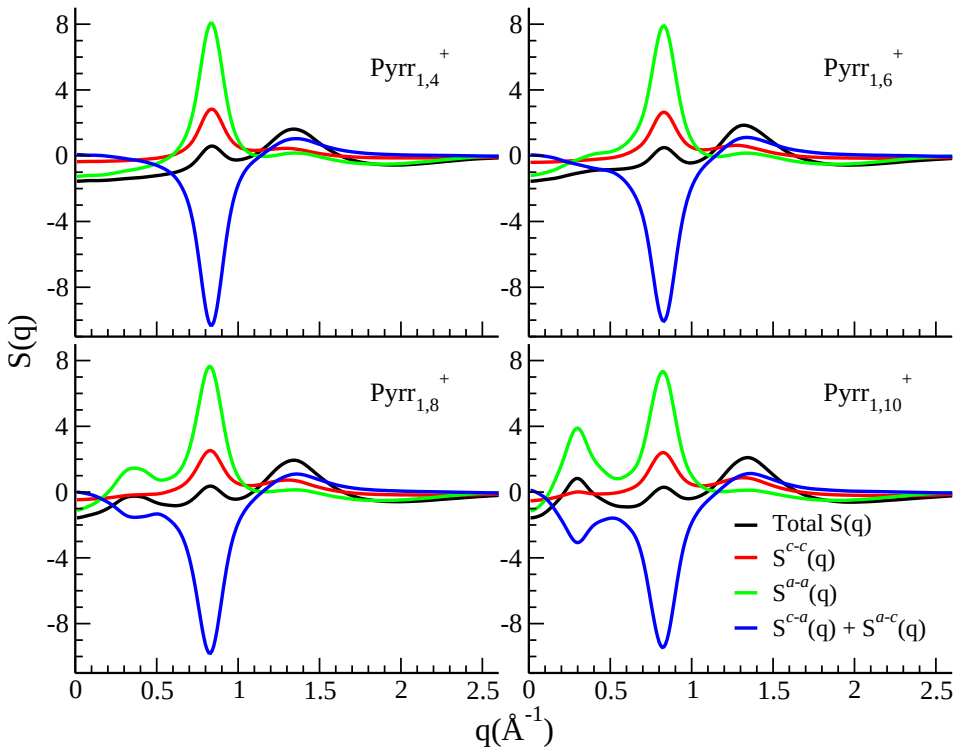

Figure 2.3: S(q) (*black*) of $Pyrr_{1,n}{}^{+}NTf_2{}^{-}$ RTILs partitioned into cation-cation (*red*), anion-anion (*green*) and cation-anion (*blue*) subcomponents.

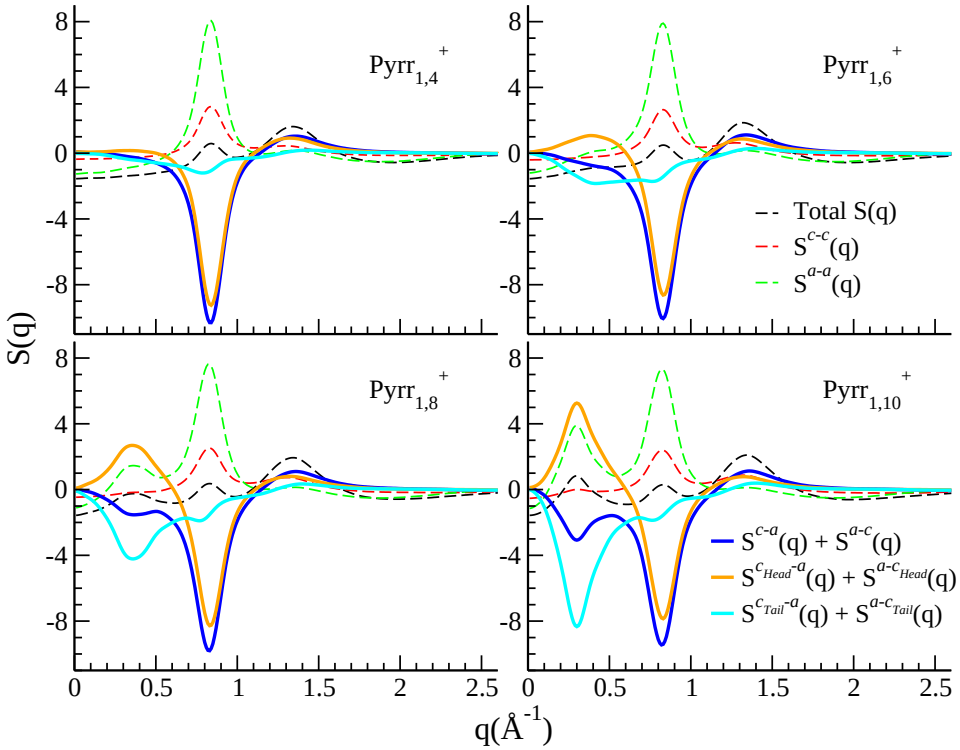

Figure 2.4: S(q) (*black*) of $Pyrr_{1,n}{}^{+}NTf_2^{-}$ partitioned into cation-cation (*red*), anion-anion (*green*) and cation-anion (*blue*). The cation-anion term is further split into cation(Head)-anion (*orange*) and cation(Tail)-anion (*cyan*) terms.

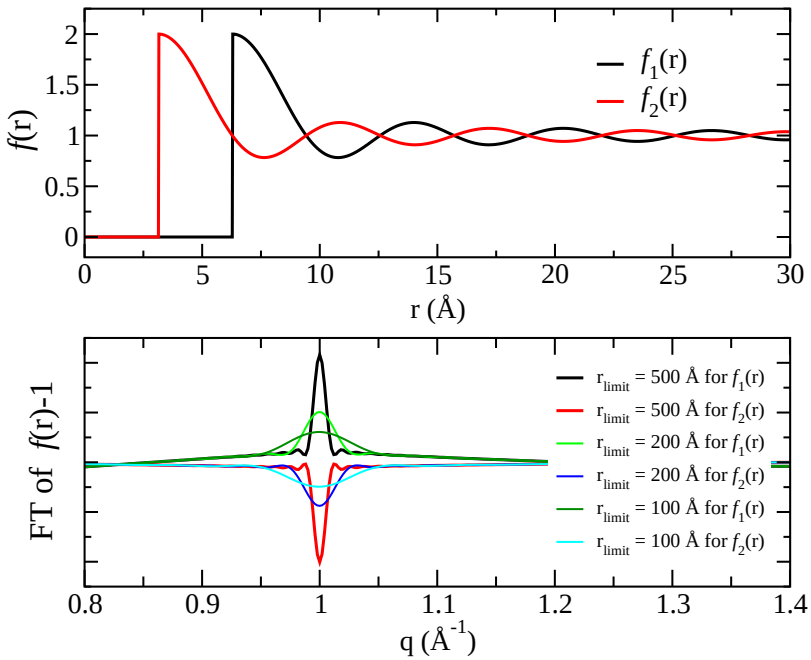

Figure 2.5: *Top*: Idealized single spatial periodicity rdf functions f(r) defined as $1 + \sin(k(r - r_0))/(k(r - r_0))$ for $r > r_0$ and zero otherwise. In all cases, $k = 1$ Å^{-1}. r_0 is set to $2\pi/k$ and π/k for f_1(r) and f_2(r), respectively. *Bottom*: The 3D Fourier transforms (FT) of f(r) corresponding to an idealized single wavenumber SAXS S(q). Since f(r) is infinitely periodic the FT is a function of the upper integration limit, r_{limit}. In the case of liquids, g(r) looses correlations after a few oscillations and therefore peaks in S(q) appear to be broad. This figure shows that f(r) functions of the same spatial periodicity but with a π spatial phase offset result in peaks and anti-peaks in reciprocal space.

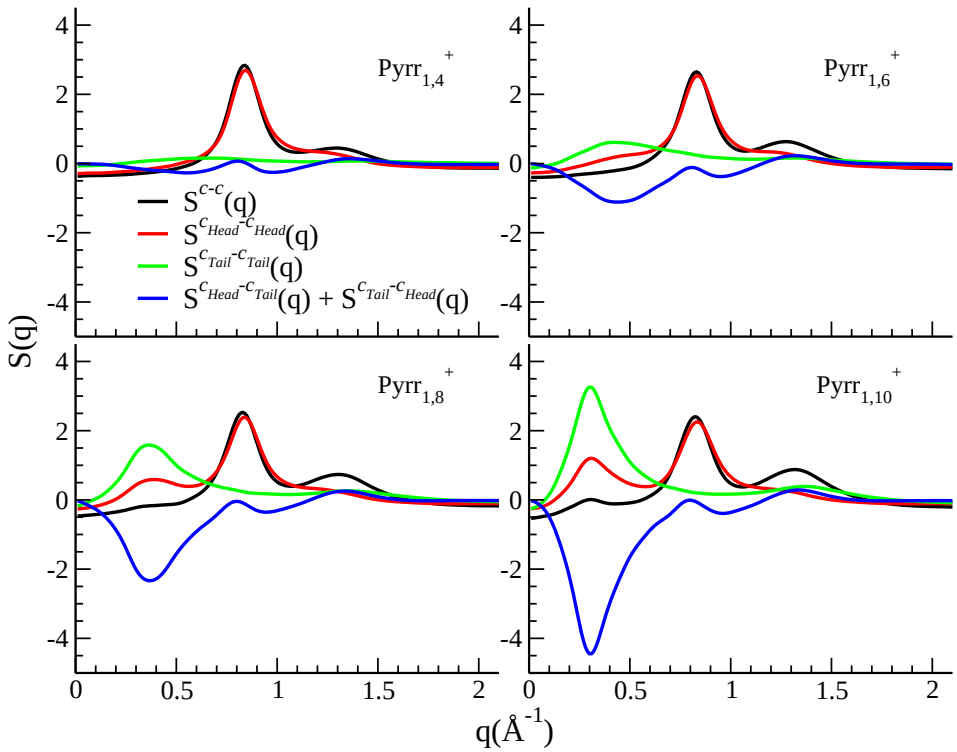

Figure 2.6: Cation-cation (*black*) S(q) partioned into Head-Head (*red*), Tail-Tail (*green*) and Head-Tail (*blue*) subcomponents.

the overall peak. Simply put this is the length scale of close contact interactions. For all RTILs studied here, and many others we have previously studied[1, 53], positive-negative charge adjacency contributes to this peak and when n is large, hydrophobic contributions become important as well.[78]

(2) The peak in S(q) at around q = 0.85 Å^{-1} is really the combination of a peak and an anti-peak. Peaks and anti-peaks at identical wavenumber happen because two spatial features have the same periodicity but different phase. In Fig. 2.5 we show that the 3D Fourier transform of Sinc (r) functions mimicking single spatial periodicity RDFs that are phase shifted give rise to such peaks and anti-peaks. Simply put, cation-cation and anion-anion densities have a common block of frequencies that are in phase. For both species, enhancements in density appears at similar distances and so do depletions. On the other hand cation-anion densities also share the same common block of frequencies but are phase shifted with respect to that of cation-cation and anion-anion. In other words when same-ion density shows an enhancement, different-ion density shows a depletion and *vice versa*. Same-ion $\mathrm{S}^{a-a}(q)$ and $\mathrm{S}^{c-c}(q)$ contributions give rise to a peak in the overall $\mathrm{S}(q)$ whereas $\mathrm{S}^{a-c}(q)$ and $\mathrm{S}^{c-a}(q)$ give rise to the anti-peak at around q = 0.85 Å^{-1}. The partitioning in Fig. 2.4 (orange line) also reinforces the notion that, the main culprit for the anti-peak at q = 0.85Å^{-1} is the correlation between the charged cationic heads and the anions, exposing the alternating charge nature of these systems.

(3) For cations with $n = 8$ and $n = 10$ a prepeak and an anti-prepeak can also be observed at q = 0.35 Å^{-1}. The onset of a prepeak and an anti-prepeak is

also present when $n = 6$. These prepeaks and anti-prepeaks correspond to a type of structural arrangement occurring on a longer lengthscale than charge alternation. In this case, in sync are the polar-polar and apolar-apolar densities and out of sync are the polar-apolar densities. This can be clearly appreciated from Fig. 2.4 and Fig. 2.6. Anion-anion correlations, cation head-anion correlations as well as cation head-cation head correlations all have positive contributions to the prepeak. This is the polar-polar contribution to the prepeak. Tail-tail correlations in cations with $n = 6$, $n = 8$ and $n = 10$ are major positive contributors to the prepeak. This is the apolar-apolar contribution to the prepeak. In contrast to these positive contributions to S(q) we have cation tail-anion (see Fig. 2.4) and cation head-cation tail (see Fig. 2.6) contributing to the anti-prepeak. In brief, prepeak and anti-prepeak reveal the lengthscale of polar/apolar alternation in these RTILs.

2.3 Conclusions

In conclusion, peaks and antipeaks correspond to spatial features of the same periodicity but with a phase offset. Or in other words, peaks and anti-peaks at the same wavenumber are signatures of some type of alternation. In the case of the pre-peak and anti-prepeak what is in phase is the polar-polar and apolar-apolar densities. What is out of phase is the polar-apolar density. In the case of the intermediate peak what is in phase is the positive-positive and negative-negative densities. What is out of phase is the positive-negative and negative-positive densities.

CHAPTER 3
ANIONS, THE REPORTERS OF STRUCTURE IN IONIC LIQUIDS IN X-RAY SCATTERING EXPERIMENTS.

3.1 Introduction

It is well established that because of their amphiphilic nature and their often larger size, cations play a fundamental role in determining the topography of ILs. In the work discussed in the current chapter, the role that different anions play in X-ray scattering experiments is unraveled. We find that it is often atoms in the anions that display the largest X-ray form factors and therefore play a very significant role as reporters of structure in X-ray scattering experiments. For a set of liquids with similar topological landscape, how does S(q) change when the anionic scattering is deemphasized? Also, how do we computationally recover the typical length scale of important and perhaps universal IL structural features such as charge alternation when these are experimentally inaccessible from S(q) because of interference cancellations? The main focus of this chapter will be on addressing these questions using the same quaternary ammonium cation coupled to three different anions, namely I^-, $PF_6{}^-$ and $N(CN)_2{}^-$.

As discussed in Chapter 2, the presence of positive and negative going partial contributions to S(q), what we call peaks and anti-peaks,[55, 56] indicative of charge alternation[53, 56, 1] and polarity alternation[55, 56] complicates the inter-

*A portion of this chapter is reproduced from The Journal of Physical Chemistry Letters. vol. 4, page 105-110, year 2013 by J.J. Hettige, H. K. Kashyap, H. V. R. Annapureddy, and C. J. Margulis. Copyright - Appendix A, DOI: 10.1021/jz301866f

pretation of experimental data because of almost complete cancellations concealing important intermediate and long range structure. Another factor complicating our understanding of these systems is that whereas cations are often the largest species providing both polarity variation and asymmetry, it is often the anions which are smaller and less topologically rich, that are the most important reporters in X-ray experiments.[56, 1, 78] An example of this is the typical pattern that bis (trifluoromethylsulfonyl)amide (NTf_2^-) containing liquids show at low q range. In general it does not appear to matter whether one is dealing with phosphonium,[79, 78, 80] imidazolium,[79, 81, 82, 1, 83, 84] alkylammonium,[79, 53] piperdinium[81] or pyrrolidinium[56, 85, 2] based systems; saving important details, so long as the anion is NTf_2^-a similar scattering pattern can be observed in the intermolecular region. The longer range organizational role of cations is often de-emphasized in S(q) and must be interpreted not only from their own self scattering, but most importantly, indirectly from the large scattering of anions as well as from cross cationic-anionic terms. It is therefore interesting to examine how enhancing the role of cations by choosing more poorly scattering anions affects S(q) and therefore our intuitive interpretation of structure, in terms of adjacency, charge alternation and polarity alternation.[56, 78]

In this work we compare the role that different anions play in the S(q) for a set of liquids with the same cation, and it is well established that because of their amphiphilic nature and their often larger size, cations play a fundamental role in the structural landscape of ILs. Describing how these familiar features change in a liquid in which scattering is not dominated by anions is one of the objectives of this

work. A second objective is to define an accurate descriptor of multiple length scale alternations that does not suffer from the cancellations concealing this information in the experimental S(q) function. To achieve these goals we compare a set of systems with a significant degree of morphological similarity in the liquid phase but with anionic X-ray form factors that are significantly different.

We have chosen three anions, I^-, $PF_6^-$and $N(CN)_2^-$while keeping the tetrapentylammonium $N^+_{5,5,5,5}$cation the same in all cases. Parameters given in references[86, 69, 87] were used for creating the force field for each system containing 1000 ion pairs. The target temperatures for $N^+_{5,5,5,5}N(CN)_2^-$, $N^+_{5,5,5,5}PF_6^-$and $N^+_{5,5,5,5}I^-$systems were set to 350 K, 600 K and 480 K, respectively. These temperatures were chosen in an attempt to run the three systems at a similar thermodynamic state about 70 K above their respective melting temperatures at ambient pressure. The melting point of the Iodide liquid is 407 K.[88] The melting point of $N^+_{5,5,5,5}PF_6^-$is not known, however that of $N^+_{3,3,3,3}PF_6^-$is reported to be 510 K [89] and that of $N^+_{4,4,4,4}PF_6^-$is reported to be in the range 517-519 K.[90] From this data we estimated the melting point of $N^+_{5,5,5,5}PF_6^-$to be around 530 K. The melting temperature of $N^+_{5,5,5,5}N(CN)_2^-$is not known either but that of $N^+_{5,5,5,5}NTf_2^-$is 298 K[91] and it is known from the work of MacFarlane and coworkers that $N(CN)_2^-$liquids often have lower melting points by about 20-30 K[92] therefore we have estimated the melting point of $N^+_{5,5,5,5}N(CN)_2^-$to be about 280 K. This number is reasonable given that the similar but asymmetric $N^+_{6,4,4,4}N(CN)_2^-$melts at 230 K.[92]

As the final production/equilibration run, each system was run for 4 ns with

full atomic charges and at target temperature and pressure in NPT ensemble. In this study we split the total S(q) into subcomponents.[56, 53, 55] For this we define the polar cationic head as consisting of the nitrogen and the first two methylene groups adjacent to it in each alkyl tail. A minor caveat is that even though these systems are made of ions the form factors are those of atoms. This is common practice in the literature since one does not have access to form factors for atoms with partial ionic charges. However the form factor for iodide is available and we used it instead of that for the iodine atom. A comparison of the liquid S(q) using ionic and atomic form factors for this anion shows only small differences at very low q values.

3.2 Results and Discussion

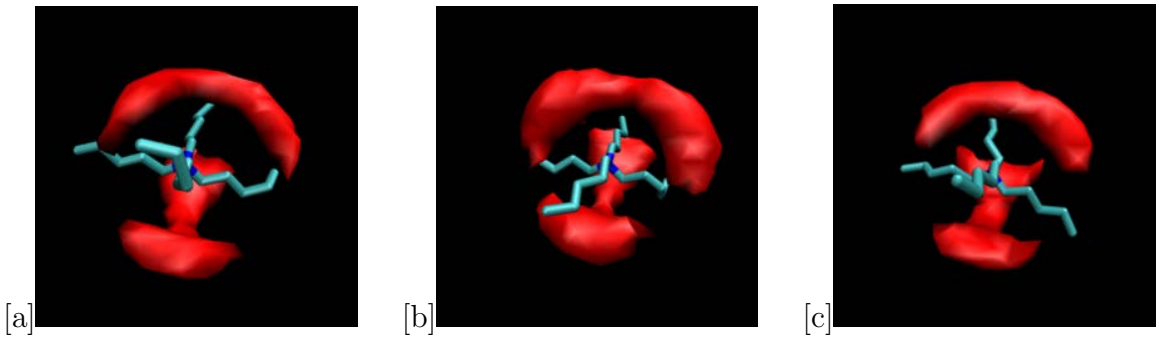

Figure 3.1: Spatial distribution functions (SDF) of anion atoms around cations in: (a)$N^{+}_{5,5,5,5}I^{-}$(b)$N^{+}_{5,5,5,5}PF_6{}^{-}$(c) $N^{+}_{5,5,5,5}N(CN)_2{}^{-}$. In each case, isovalues were chosen to reflect the first solvation shell. This shell appears as perpendicular bands on opposing sides of the cation.

Figure 3.1 shows the overall distribution of anion atoms around the $N^{+}_{5,5,5,5}$ cation for the three liquids studied. It is clear from Fig. 3.1 that anionic distributions around the cation are qualitatively very similar in all three liquids. In all cases anions appear to form two perpendicular bands above and below the cation.

This qualitative similarity can also be observed in the radial distribution functions (RDF) in Fig. 3.2. All three systems show central atom RDF that are qualitatively similar with differences in peak positions that are a result of different anionic volumes. In the case of the $N(CN)_2^-$containing system the cation-anion first peak shows a double feature most likely due to the non-spherical geometry of the anion.

Based on the real space representations of liquid structure in Fig. 3.1 and Fig. 3.2 one would perhaps expect similar S(q) functions. Figure 3.3 shows a comparison of the S(q) for the three systems studied. Interestingly all three systems appear to show two peaks, the prepeak at around 0.5 $Å^{-1}$ and the adjacency peak at around 1.5 $Å^{-1}$ but not an obvious intermediate peak at around 0.8 $Å^{-1}$ associated with charge alternation.[53, 56, 1, 78] We will show below that this is not because charge alternation is missing in these systems, but instead because of almost complete cancellation of peaks and anti-peaks that conceal this important short length scale ordering. Another interesting observation stemming from the poor scattering nature of the $N(CN)_2^-$anion is that the adjacency peak but more importantly the prepeak is less pronounced than in the other two systems in which the anionic scattering is much stronger. Basically, the magnitude of peaks in S(q) in systems that are topologically quite similar can appear to be significantly different when the weight of

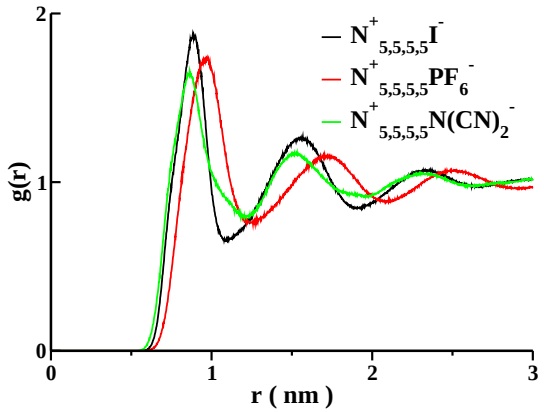

[a]

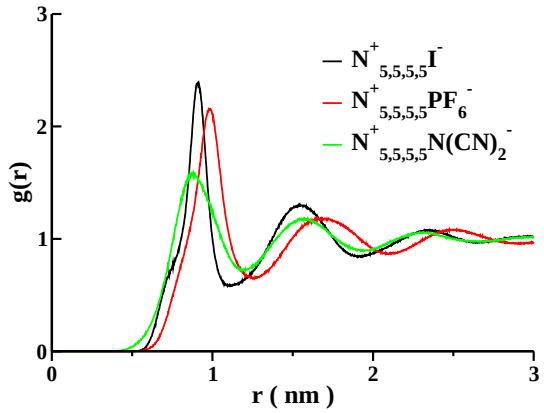

[b]

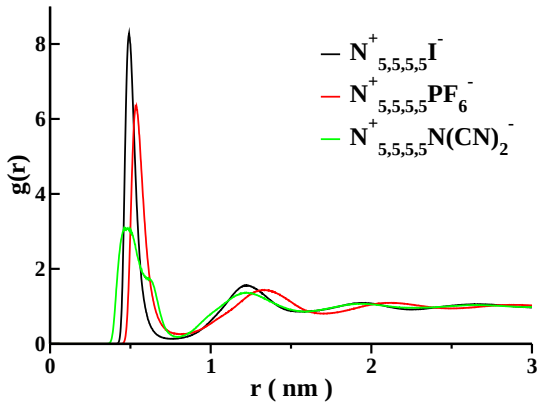

[c]

Figure 3.2: Radial distribution functions between (a) cation-anion central atoms (b) anion-anion central atoms (c) cation-cation central atoms. Simulation temperatures for the$N^{+}_{5,5,5,5}N(CN)_2^{-}$, $N^{+}_{5,5,5,5}PF_6^{-}$and $N^{+}_{5,5,5,5}I^{-}$systems were 350 K, 600 K and 480 K, respectively.

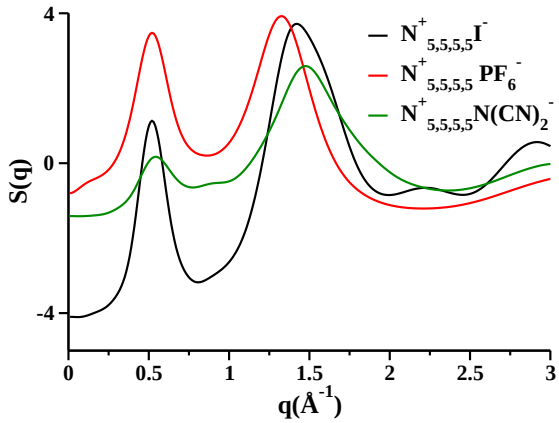

Figure 3.3: Comparison between total structure functions S(q) of $N^{+}_{5,5,5,5}I^{-}$at 480 K, $N^{+}_{5,5,5,5}PF_6^{-}$at 600 K and $N^{+}_{5,5,5,5}N(CN)_2^{-}$at 350 K.

anionic scattering is diminished. Figure 3.4 sheds light on several structural aspects of this liquid series. First it is clear that in all three liquids the intermediate peak indicative of charge ordering is missing strictly because of cancellations and not because this ordering is not present. In fact the peaks and anti-peaks at around 0.8 $Å^{-1}$ are very pronounced indicating significant structural alternation at this q value. Second, Fig. 3.4 shows that the role of the anion as a reporter of structure in the $N(CN)_2^{-}$containing liquid is significantly diminished. The anion-anion subcomponent is of significantly less amplitude when compared to the other two systems and so is the amplitude of the cation-anion alternation anti-peak at around 0.8 $Å^{-1}$. The opposite is true for the purely cationic component which is comparable in amplitude in all three systems. Figure 3.4 exemplifies how by adjusting the anionic scatter-

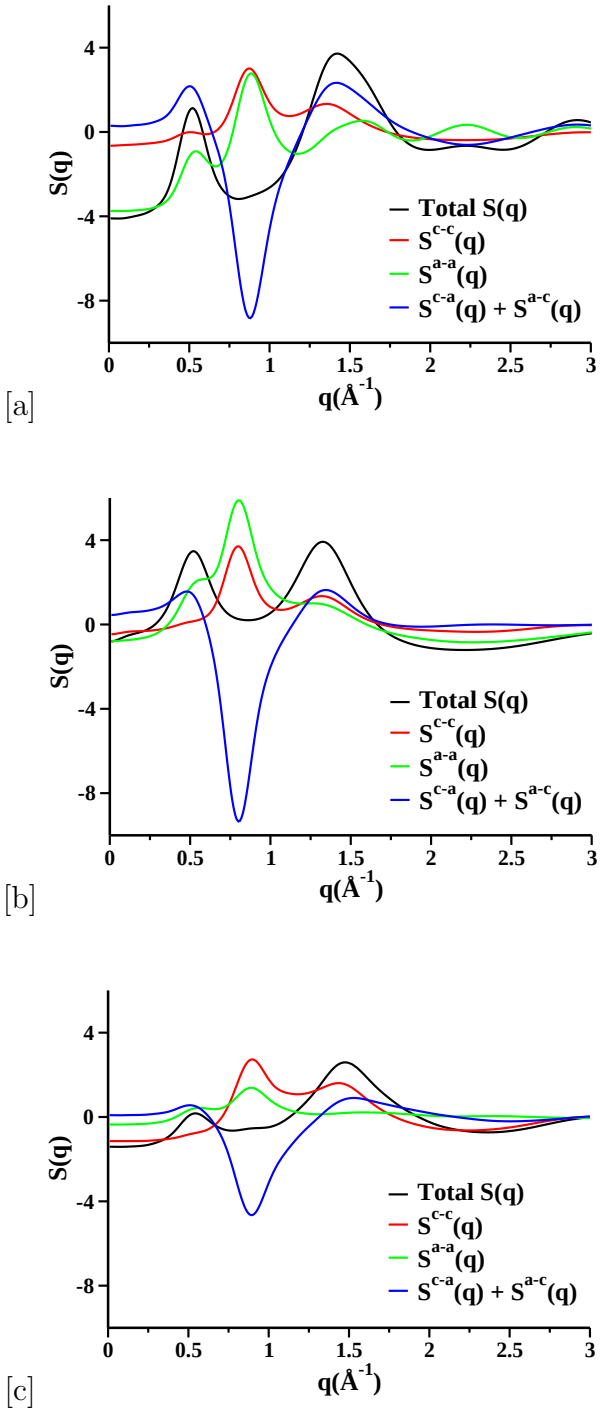

Figure 3.4: Total and partial structure functions (cation-cation, anion-anion, cation-anion + anion- cation) S(q) of (a) $N^{+}_{5,5,5,5}I^{-}$(b) $N^{+}_{5,5,5,5}PF_6^{-}$(c) $N^{+}_{5,5,5,5}N(CN)_2^{-}$. Simulation temperatures for $N^{+}_{5,5,5,5}N(CN)_2^{-}$, $N^{+}_{5,5,5,5}PF_6^{-}$and $N^{+}_{5,5,5,5}I^{-}$were 350 K, 600 K and 480 K, respectively.

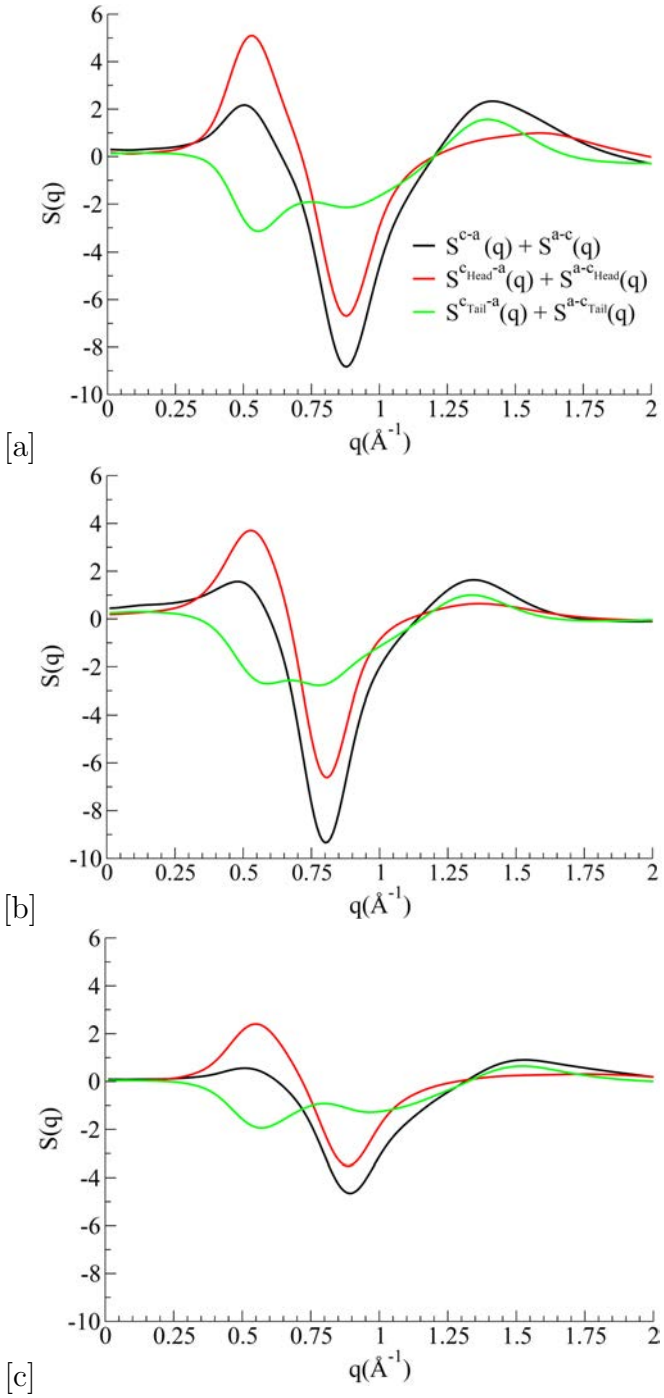

Figure 3.5: Cation-anion S(q) (black) partitioned into cation head-anion (red) and cation tail-anion (green) for (a) $N^{+}_{5,5,5,5}I^{-}$(b) $N^{+}_{5,5,5,5}PF_6^{-}$(c) $N^{+}_{5,5,5,5}N(CN)_2^{-}$.

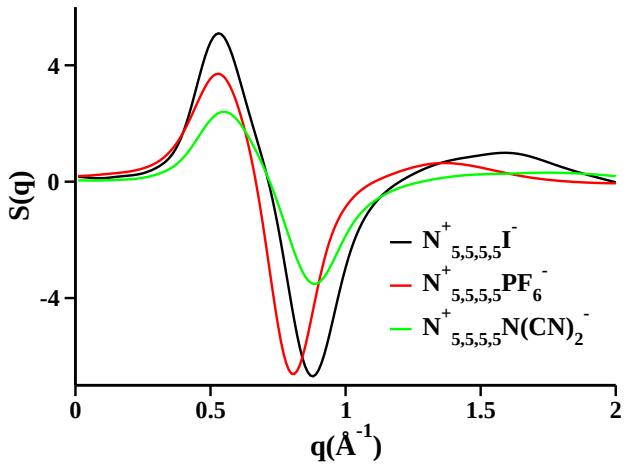

Figure 3.6: Cation head anion S(q) of $N^{+}_{5,5,5,5}I^{-}$, $N^{+}_{5,5,5,5}PF_6^{-}$and $N^{+}_{5,5,5,5}N(CN)_2^{-}$. The peak at low q identifies the inverse length scale for polarity alternation and the antipeak at about 0.8 $Å^{-1}$ identifies the inverse length scale for charge alternation. Simulation temperatures for $N^{+}_{5,5,5,5}N(CN)_2^{-}$, $N^{+}_{5,5,5,5}PF_6^{-}$and $N^{+}_{5,5,5,5}I^{-}$were 350 K, 600 K and 480 K, respectively.

ing weight one is able to better highlight cationic scattering features in the overall S(q). Further evidence of the diminished role of the anion in the scattering of the $N(CN)_2^-$containing liquid can be observed in Fig. 3.5 where cation head-anion, cation tail-anion and total cation-anion subcomponents are compared across systems.

The reader is reminded that alternations on different length scales are characterized by peaks and anti-peaks[55, 56, 78] in the subcomponents of S(q) which in cases can perfectly cancel. The phenomenon of cancellation of the charge alternation peak in S(q) shown in Fig. 3.3 at about 0.8 $Å^{-1}$ is not particular to this group of systems but instead is generic behavior in many other ILs.[78] Perhaps the prepeak which often corresponds to polarity alternation may also be missing in some systems because of fortuitous cancellations. Finally there may be systems in which the intermediate charge alternation feature may overlap to some extent with the low q prepeak. How can one easily and consistently extract from computer simulations the characteristic length scales for charge and polarity alternations in systems where these are concealed from X-ray experiments? The answer to this is given in Fig. 3.6 If one plots the cation polar head-anion subcomponent of S(q) this should always result in a negative going peak (an anti-peak) in the intermediate charge alternation region. We remind the reader[78] that positive-positive charge contributions give rise to peaks at this intermediate range while positive-negative charge contributions give rise to anti-peaks in this region. By the same token, the cation polar head-anion subcomponent of S(q) gives rise to a positive going peak at the prepeak position. This is because in the prepeak region, polar-polar type interactions give rise to pos-

itive going peaks whereas polar-apolar type interactions give rise to negative going peaks (anti-peaks).[56] Therefore plotting this function and finding the anti-peak at intermediate q range identifies the inverse length scale for charge alternation. Instead finding the position of the peak in this function at low q range identifies the inverse characteristic distance for polarity alternation. This function identifies both length scales even when there are complete cancellations in the prepeak or the intermediate charge alternation peak in the overall computational or experimental structure function S(q).

3.3 Conclusions

In conclusion, for most room-temperature ILs, in X-ray experiments anions have a very important role as reporters of structure. This is not necessarily the case when the anion is poorly scattering such as dicyanamide. Many ILs, particularly those with long non-polar alkyl tails, have three different length scales of organization; adjacency interactions, charge alternation and polarity alternation. However in some cases at least one of these alternations is completely or nearly completely absent from the experimental S(q). This is because of cancellations of peaks and anti-peaks in subcomponents of S(q). One way to recover the missing information about length scales for charge and polarity alternation is to plot computationally derived cation head-anion partial S(q) functions. The position of the peak at low q and anti-peak at intermediate q values in this function correlates to polarity alternation and charge alternation characteristic inverse distances respectively. This analysis should be valid

for all common ILs in which alkyl tails are on the cations not on the anions.

CHAPTER 4
ANOMALOUS TEMPERATURE DEPENDENCE OF THE NANOSCALE STRUCTURE OF PHOSPHONIUM IONIC LIQUIDS.

4.1 Introduction

From what we have discussed so far, it is clear that the prepeak is a corollary of the nanoscale organization present in many ILs. During the last decade a significant portion of the physical chemistry literature on RTILs has focused on this intermediate range order of ILs at the nanoscale level.[93, 85, 94, 95, 96]. It is intriguing to better understand how such nanoscale structure is affected by temperature. A few studies have been carried out on the behavior of the prepeak with temperature[97, 98]. For some ILs, temperature dependent X-ray scattering studies have shown that the prepeak -indicative of polar-apolar alternation- decreases in intensity as temperature is increased in the liquid phase. This is because, the intermediate nanoscale organization diminishes at higher temperature. However, the X-ray scattering experiments and computer simulations carried out by the Castner and Margulis groups[78] have recently observed that the opposite is true in the case of the popular tetradecyltrihexylphosphonium bis(trifluoromethylsulfonyl)amide ([$P_{14,6,6,6}$][NTf_2]) IL. In here, the intensity of the prepeak shows a counter intuitive behavior as the prepeak intensity increases with increasing temperature.

Therefore, the purpose of this study is to give an interpretation to the anoma-

---

*A portion of this chapter is reproduced from The Journal of Chemical Physics. vol. 140, page 111102, year 2014 by J.J. Hettige, H. K. Kashyap, and C. J. Margulis. Copyright - Appendix B, http://dx.doi.org/10.1063/1.4867900

lous behavior observed experimentally and computationally at the smallest scattering vectors corresponding to the prepeak region in the case of popular tetradecyltrihexylphosphonium based ionic liquids.

What we attempt to demonstrate in the current chapter is that the anomalous increase in intensity of the prepeak is associated with a loss in apolar-apolar organization at higher temperatures, with modest implications to S(q), that is counterbalanced by a gain in polar-polar ordering with important implications in S(q). In other words, at lower temperatures the long nature of the alkyl tails in the cation results in apolar ordering at the expense of less well organized polar components. Loss in apolar order at higher temperatures appears to allow for better polar organization. Since anions are often the reporters of structure in ionic liquids,[99] a loss of organization of the apolar component at higher temperature coupled with better organization of polar components gives rise to a prepeak of higher intensity.

The number of ions (1000 ion pairs) used for the study discussed in this chapter is more than three times that in the recent article[78] in which we compared for the same system experimental vs. computational structure functions. This increase allows us to get better statistics at low q values. The results however are consistent with our prior simulations and experimental data. The Optimized Potentials for Liquid Simulations All-Atoms (OPLS-AA)[49, 48] and Lopes-Pádua[69, 86] force field parameters were employed to model the system for simulations. Then the system with full atomic charges was run for about 5.5 ns while raising and lowering the temperature to achieve proper equilibrium at the desired temperatures and 1 bar

pressure. Thereafter, the system was let to equilibrate for about 6.0 ns at each temperature. Hence in all the cases, simulations were run for at least 11 ns. Equation 1.7 was used to calculate the structure function S(q) of the system at 225 K, 295 K, 353 K and 400 K temperatures.

4.2 Results and Discussion

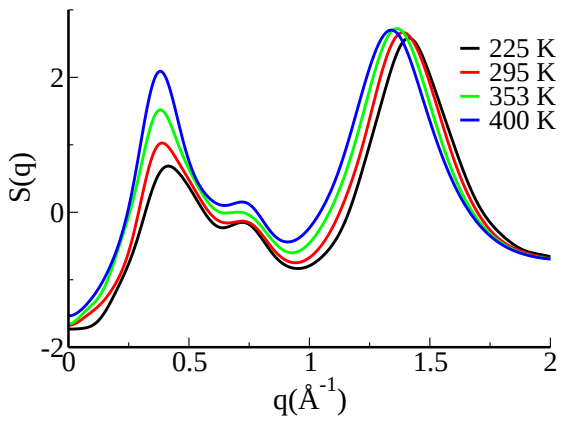

Figure 4.1: Comparison between structure functions S(q) of $[P_{14,6,6,6}][NTf_2]$ at different temperatures.

Figure 4.1 shows computationally derived S(q) for $[P_{14,6,6,6}][NTf_2]$ at temperatures ranging from 225 K to 400 K. Two most important facts can be derived from this figure; all peaks move to smaller q values as temperature is increased and the intensity of the prepeak below 0.5 Å^{-1} significantly increases with temperature. The

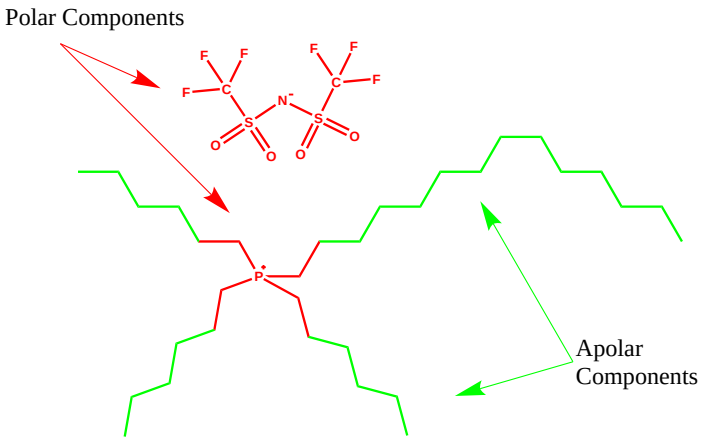

Figure 4.2: Definition of group partitions for $[P_{14,6,6,6}][NTf_2]$ as used in this chapter.

shift to smaller q values is likely a trivial consequence of volume expansion. The increase in intensity of the prepeak with temperature deserves careful scrutiny.

In a recent article[55] we explained how S(q) could be mathematically partitioned into polar-polar contributions, apolar-apolar contributions and corresponding polar-apolar terms. This type of partitioning of S(q) is exactly what is required to explain the anomalous behavior of the prepeak in $[P_{14,6,6,6}][NTf_2]$. The definition of polar and apolar groups for the $[P_{14,6,6,6}][NTf_2]$ ionic liquid is depicted in Fig. 4.2.

In this chapter, we will show that it is the purely polar component which is the most important contributor to the anomalous behavior of the prepeak intensity with temperature.

We analyze first the minor contribution of the apolar subcomponent. Apolar subcomponents are important in two very different regions in S(q). At higher q values around 1.4 $Å^{-1}$ (see Fig. 4.1) the apolar subcomponent gives rise to adjacency corre-

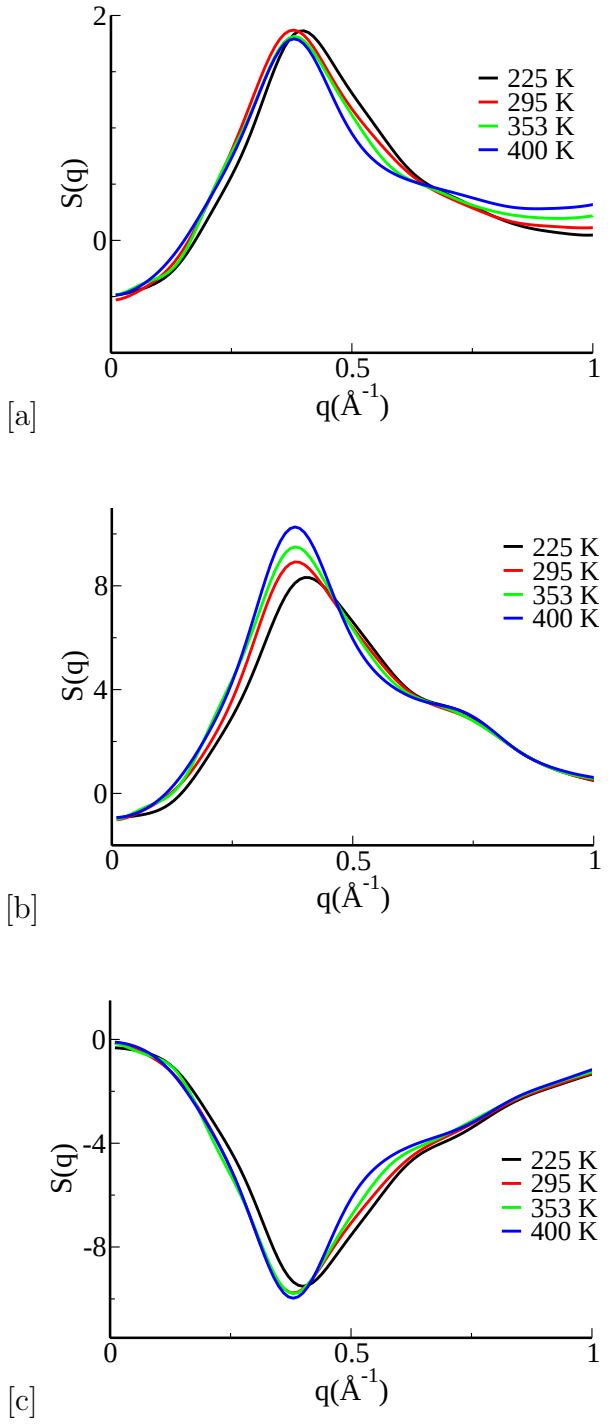

Figure 4.3: (a)Apolar-apolar, (b) polar-polar and (c) polar-apolar components of S(q) for $[P_{14,6,6,6}][NTf_2]$at different temperatures.

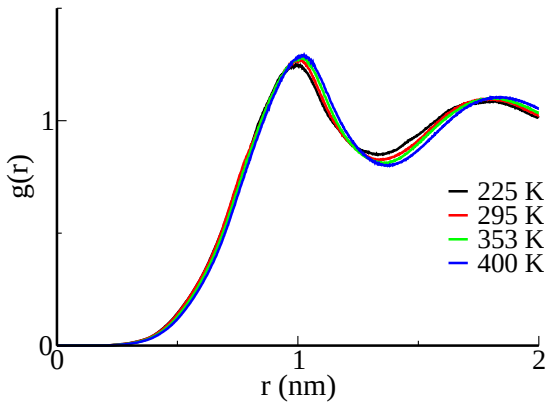

[a]

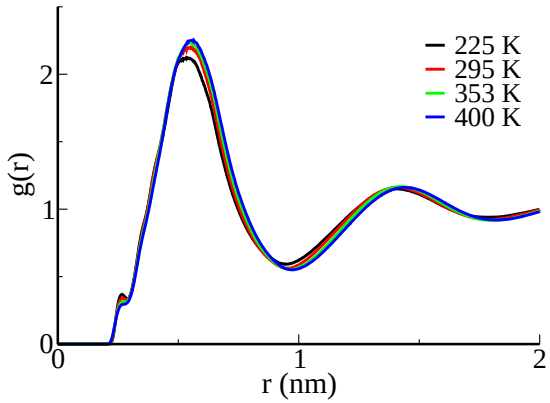

[b]

Figure 4.4: Radial Distribution Functions between (a) cation head-head (intermolecular) and (b) cation head-anion for $[P_{14,6,6,6}][NTf_2]$ at different temperatures.

lations which are both intramolecular as well as nearest neighbor in nature. Apolar correlations also contribute to the prepeak below 0.5 Å^{-1}. We have demonstrated in previous articles[1, 78, 100, 101, 99, 53, 56, 55] that this reflects the typical inverse length scale between apolar regions separated by polar regions. In other words this is the typical inverse length scale that separates groups of tails that are not adjacent but instead have polar cationic heads or anions between them. Figure 4.3 a) shows that the intensity behavior of this apolar prepeak is just as expected. In general, lower temperature induces a higher degree of intermediate order and a more intense prepeak.

The situation of the apolar component in Fig. 4.3 a) should be contrasted against that of the polar component. The purely polar component of S(q) depicted in Fig. 4.3 b) shows exactly the opposite pattern for the intensity of the prepeak as a function of temperature. In Fig. 4.3 b) , the prepeak grows as temperature increases. What this means is that whereas increasing the temperature implies a loss of order for the apolar component it implies gains at the same scattering vector value for the polar component. The reader is reminded that the prepeak is also associated with the typical inverse length scale between charged components that are not adjacent and instead are separated by apolar tails.[1, 55, 56]

An important result that must be emphasized is that independent of temperature the overall intensity of the polar-polar contribution to the prepeak is always much higher than the corresponding apolar-apolar contribution. Similarly, the changes in peak intensity with temperature at the prepeak position are much more pronounced

for the polar-polar component than for the apolar-apolar component. We have explained in a recent article[99] that this is simply because in most cases, the anions are the most scattering components and therefore the *de facto* reporters of structure.

Figure 4.3 c) shows the polar-apolar contribution to S(q) at the prepeak region. It is expected that this contribution will be negative going. We have mathematically proven this in previous articles.[55, 56] The physical reason for this is that the polar-apolar correlation has the same periodicity as the polar-polar and apolar-apolar components but is shifted in origin. Upon Fourier transformation this gives rise to a feature at the same q value but with a phase shift that makes it negative going in nature. One expects that the temperature dependence of this cross term will be complex since it has to reflect both the higher order of polar components at high temperature but also the higher order of apolar components at low temperature. Therefore, there are two competing effects. In any case, the difference in intensity values as a function of temperature for the polar-apolar component is not significant when compared to that of the polar-polar component which dominates the sum of polar-polar + apolar-apolar + polar-apolar contributions to the prepeak. Since polar-polar, apolar-apolar and polar-apolar contributions are additive, the increase of polar-polar contribution with temperature at the q value for the prepeak simply overwhelms all other contributions.

Features in S(q) are not associated with any single peak in real space representation g(r). Nonetheless, it is instructive to look at the first peak of g(r) because it gives us information about how well organized the first solvation shell around species

or sub-components of species is. Consistent with our intuitive explanation for the anomalous phenomenon described in this chapter, Fig. 4.4 shows that the first peak in the intermolecular cationic head-head RDF as well as the cationic head-anion RDF have larger intensities as temperature increases.

4.3 Conclusions

The theory and experiments appear to indicate that $[P_{14,6,6,6}][NTf_2]$ and possibly other $P^{+}_{14,6,6,6}$ containing ILs display a set of somewhat competing packing interactions. At low temperature the apolar component dominates organization at the expense of the polar component. As temperature is increased we see what appears to be organization in the polar component at the expense of the apolar component. In principle both components affect the intensity of the prepeak in opposite directions. Based on what happens to the tails, the prepeak should go down in intensity with an increase in temperature, and based on what happens to the polar components it should go up. Since the anions are often most important as reporters of structure the gain in organization of the polar component is heavily weighted in X-ray experiments and this is why we observe an increase in intensity of the prepeak with an increase in temperature.

CHAPTER 5
NANOSCALE STRUCTURE OF TETRADECYLTRIHEXYLPHOSPHONIUM BASED IONIC LIQUIDS.

5.1 Introduction

A recent feature article[102] highlights our most current understanding of ionic liquid structure based on the interpretation of X-ray scattering experiments and computer simulations. Briefly, ionic liquids are dominated by three length scales associated with short range adjacency correlations, positive-negative charge alternation and intermediate-range nanoscale polar-apolar alternation. For the tetradecyltrihexylphosphonium ($P_{14,6,6,6}{}^{+}$) cation coupled with different anions (tetrafluoroborate (BF_4^-), hexafluorophosphate (PF_6^-), chloride (Cl^-), bromide (Br^-), dicyanamide (DCA $^-$) and bis(trifluoromethylsulfonyl)amide ($NTf_2{}^-$)), it is this longest scale correlation and its temperature dependence that is the focus of the current work. The structure of anions and cations used in the study, as well as definitions of cationic 'head' and 'tail' subcomponents used in partitions of the structure function S(q) are depicted in Figure 5.1.

Several researchers have studied the structure of selected ionic liquids based on the $P_{14,6,6,6}{}^{+}$cation.[103, 80, 104, 105, 106, 54, 107] In particular, Gontrani *et al.* studied the tetradecyltrihexylphosphonium chloride IL using X-ray scattering and molecular dynamics simulations and observed the existence of nanoscale segregation.[80] As we discuss below, polar-apolar alternation giving rise to such segregation can be linked with what is commonly called a prepeak or first sharp diffraction peak in the

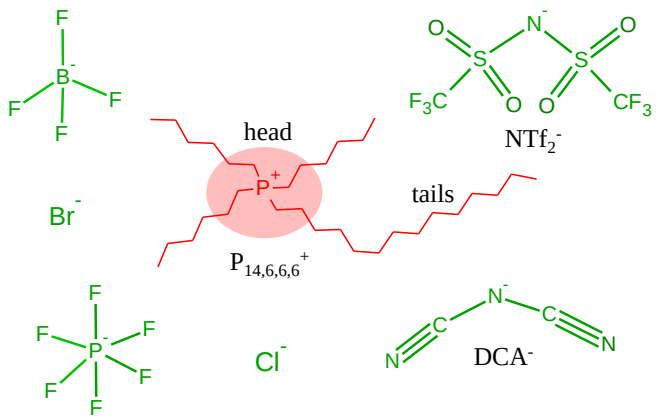

Figure 5.1: Chemical structures of the cations and anions used in this study, and the definitions of cation head and tail used to define polar and apolar subcomponents of S(q).

X-ray scattering diffraction pattern. In previous studies,[54, 107] we noticed that the dependence of the prepeak on temperature for the $P_{14,6,6,6}{}^{+}/NTf_2^{-}$ IL was at odds with that in other systems.[97, 98] The current study, will demonstrate that this is generic behavior for all studied anions when the $P_{14,6,6,6}{}^{+}$cation is included as a temperature increase always results in an intensity increase at q values associated with the prepeak.

In the study discussed in the current chapter, six phosphonium based ILs namely, $P_{14,6,6,6}{}^{+}/BF_4^{-}$, $P_{14,6,6,6}{}^{+}/PF_6^{-}$, $P_{14,6,6,6}{}^{+}/Cl^{-}$, $P_{14,6,6,6}{}^{+}/Br^{-}$, $P_{14,6,6,6}{}^{+}/DCA^{-}$and $P_{14,6,6,6}{}^{+}/NTf_2^{-}$were simulated inorder to study the temepeature dependent structure of these ILs. The OPLS-AA[48] and Canongia-Lopes & Pádua[69, 108, 109] force field parameters were used to model each system.

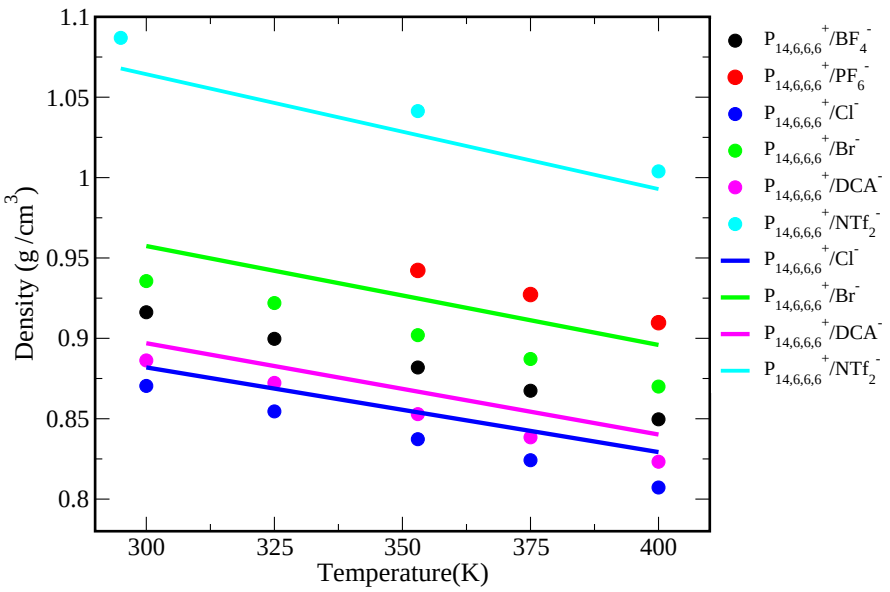

Figure 5.2: Comparison of simulated (symbols) and available experimental (lines) densities for $P_{14,6,6,6}{}^{+}$ based ionic liquids studied as a function of temperature. Available experimental data for $P_{14,6,6,6}{}^{+}/Cl^{-}$ from Ref. [3], $P_{14,6,6,6}{}^{+}/Br^{-}$ from Ref. [4], $P_{14,6,6,6}{}^{+}/DCA^{-}$ from Ref. [5], and $P_{14,6,6,6}{}^{+}/NTf_2^{-}$ from Ref. [6, 7, 8]. Data was either directly measured or interpolated/ extrapolated as needed.

As a test of the force field behavior with temperature, in Fig. 5.2 we present the computed densities as compared with available experimental data. Experimental and computational results follow similar trends with a systematic offset of about 3% which is considered acceptable.

5.2 Results and Discussion

X-ray structure functions S(q) for most typical ILs are remarkably similar; see for example figure 1 in reference [102]. In all cases, there is a signature of adjacency correlations in the region around 1.5Å^{-1} and polar-apolar alternations result in a first sharp diffraction peak below 0.5 Å^{-1}. Charge alternation manifests as a peak or shoulder at q values intermediate between these two features. In some cases, the region in S(q) corresponding to charge alternation symmetry appears almost flat. This is only because of almost perfect cancellations of what we have called peaks and antipeaks. As can be appreciated from Fig. 5.3, with subtle differences, the pattern observed for S(q) is repeated for the whole collection of $P_{14,6,6,6}{}^{+}$ based ionic liquids.

In prior work we have identified the cationic head-anionic subcomponent of S(q) as the ideal mathematical function for revealing system specific length scales associated with charge and polarity alternation in the liquid phase.[99, 100] This is because cationic head and anion belong to same-type (i.e. polar-polar) correlations in the prepeak region (low q) giving rise to a peak, but opposite-type (i.e. positive-negative) correlations in the charge alternation region (intermediate q) giving rise to

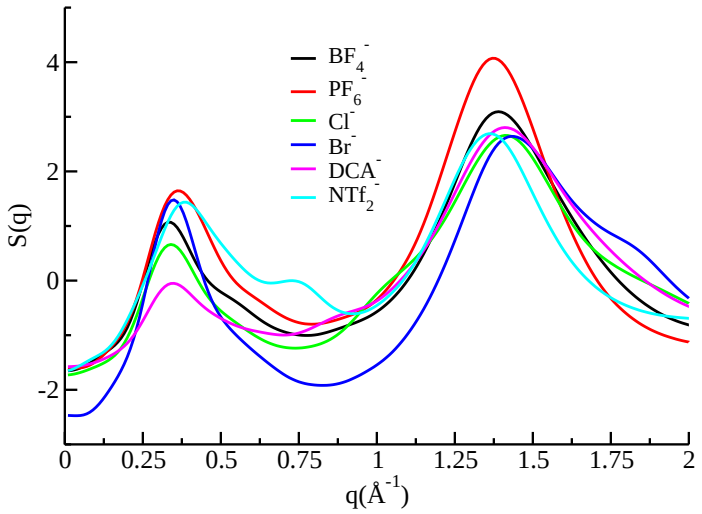

Figure 5.3: Comparison of simulated total $S(q)$ for the $P_{14,6,6,6}{}^{+}/BF_4^-$, $P_{14,6,6,6}{}^{+}/PF_6^-$, $P_{14,6,6,6}{}^{+}/Cl^-$, $P_{14,6,6,6}{}^{+}/Br^-$, $P_{14,6,6,6}{}^{+}/DCA^-$, and $P_{14,6,6,6}{}^{+}/NTf_2^-$ ILs at 353 K. All liquids show a peak in the region 1.25 to 1.75 $Å^{-1}$ corresponding to adjacency correlations, a peak below 0.5 $Å^{-1}$ characteristic of polar-apolar alternation and an intermediate region between these two associated with positive-negative charge alternation.

an antipeak. The behavior of this function is universal for prototypical ILs that display a prepeak. For the family of liquids studied here, Fig. 5.4 clearly demonstrates this and corresponding insets provide visual description of the type of alternation (polarity in red and green) and charge in (red and blue) associated with the corresponding peak (low q) and antipeak (intermediate q).

To better appreciate the sponge-like morphology of typical $P_{14,6,6,6}{}^{+}$ based

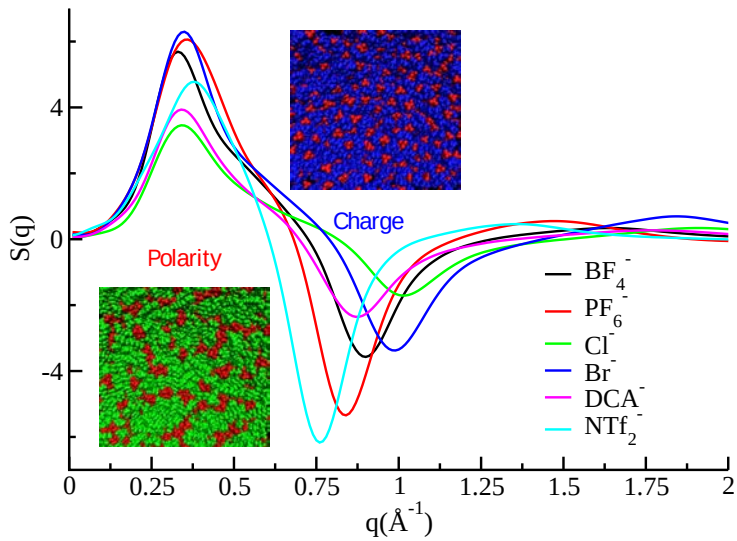

Figure 5.4: The cation head-anion partial subcomponents of S(q) for the $P_{14,6,6,6}{}^{+}/BF_4^-$, $P_{14,6,6,6}{}^{+}/PF_6^-$, $P_{14,6,6,6}{}^{+}/Cl^-$, $P_{14,6,6,6}{}^{+}/Br^-$, $P_{14,6,6,6}{}^{+}/DCA^-$ and $P_{14,6,6,6}{}^{+}/NTf_2^-$ ILs at 353 K. A peak at low q values is the signature of polar-apolar alternations whereas an antipeak in the range 0.7-1.1 $Å^{-1}$ is the hallmark for alternation of charge. Insets highlight in red and green polar-apolar alternation (green is apolar and red is polar) and in blue and red positive-negative alternation (blue is cation head and red is anion).

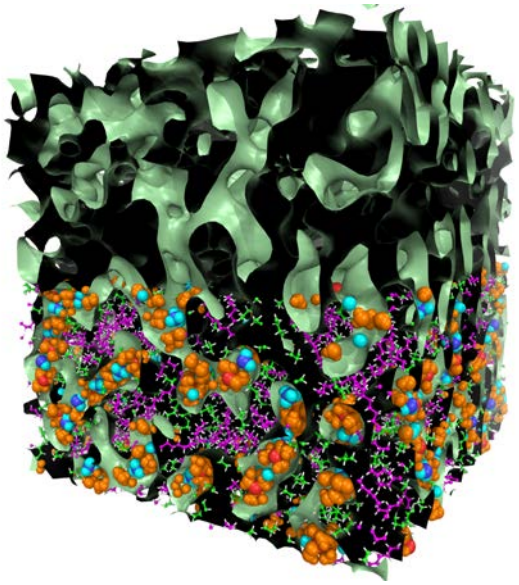

[a]

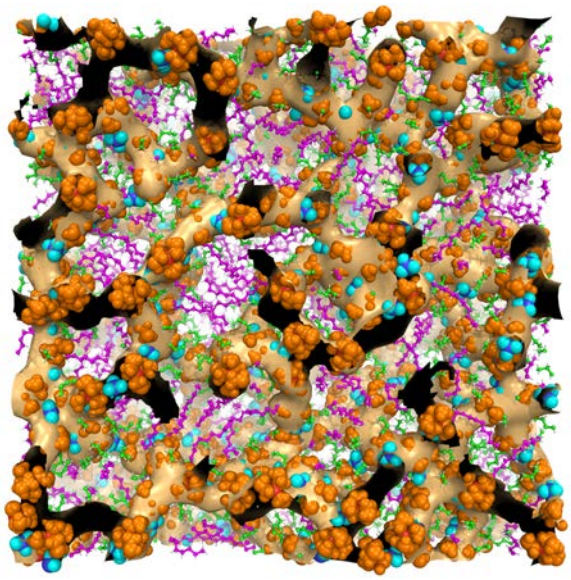

[b]

Figure 5.5: Encapsulated inside the green isosurface in Figure apolar liquid components; on the outside are charges. For visual clarity, ions are displayed only in the lower part of figure 5.5 (a). Figure 5.5 (b) shows an alternative view in which a light brown isosurface encloses a continuously percolating charge network (cation heads in brown/red and anions in dark/light blue). Short tails(green) appear to decorate this network whereas longer tails (purple) tend to define inter-strand distances. Both representations are for $P_{14,6,6,6}{}^{+}/BF_4^-$ at 375 K.

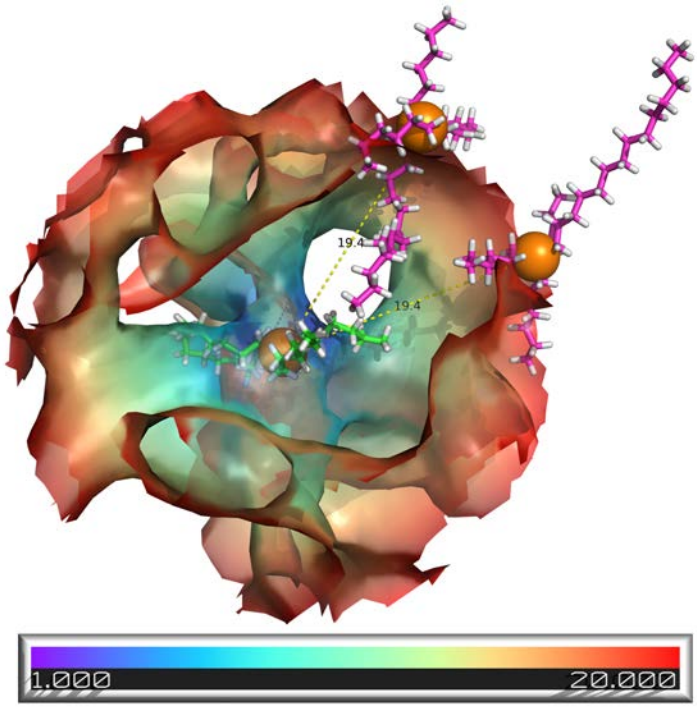

Figure 5.6: Central cation and isosurface of cations color coded by distance in the case of $P_{14,6,6,6}{}^{+}/BF_4^-$ at 300K. Highlighted are two satellite cations that in correlation with the central one have important polar-polar contributions to the prepeak.

ILs, figures 5.5(a) and (b) highlight the disordered continuously percolating network of charge and the apolar subcomponent. In particular, Fig. 5.5 (a) depicts an isosurface that encapsulates tails (green on the outside, dark in the inside) leaving outside the charge network. A complementary view of such system is given by Fig. 5.5 (b) where continuously percolating tubes (isosurface in light brown) enclose a charge network and on the outside one finds the apolar subcomponent. This figure appears to qualitatively show the six-carbon tails (short tails) decorating the charge

network whereas the long tails to some extent define the spacing between charge strings. Yet another way to identify the characteristic length scale associated with polar correlations (charge separated by the apolar subcomponents) is presented in Fig. 5.6. In this figure, a central cation surrounded by an isosurface of other cations is shown color coded by distance. Two selected satellite cations with important contributions to S(q) in correlation with the central ion are highlighted.

As opposed to other structural features that we have highlighted as universal across families of ILs, the temperature dependence of the prepeak intensity which characterizes polar-apolar periodicity can significantly differ across liquids. For some ILs, at least in the temperature range experimentally studied,[97, 98] the prepeak intensity decreases with increasing temperature. Instead, temperature dependence studies for liquids based on the $P_{14,6,6,6}{}^{+}$cation coupled with the NTf_2^{-}[54, 107] have shown the opposite behavior. Figures 5.7 highlights this behavior for all $P_{14,6,6,6}{}^{+}$-based ILs studied here. An increase in intensity of the first sharp diffraction peak with increasing temperature implies better spatial recurrence or periodicity at higher temperature in the polar-apolar alternation regime which is certainly puzzling.

What is the cause of this behavior or at least what liquid subcomponent is responsible for this? To address this question, we make use of the fact that S(q) can be partitioned into subcomponents that are additive. In particular, since we are interested in q values associated with the polarity alternation region, it is preferable to split S(q) into its polar, apolar and polar-apolar subcomponents.[56, 55, 100, 53]

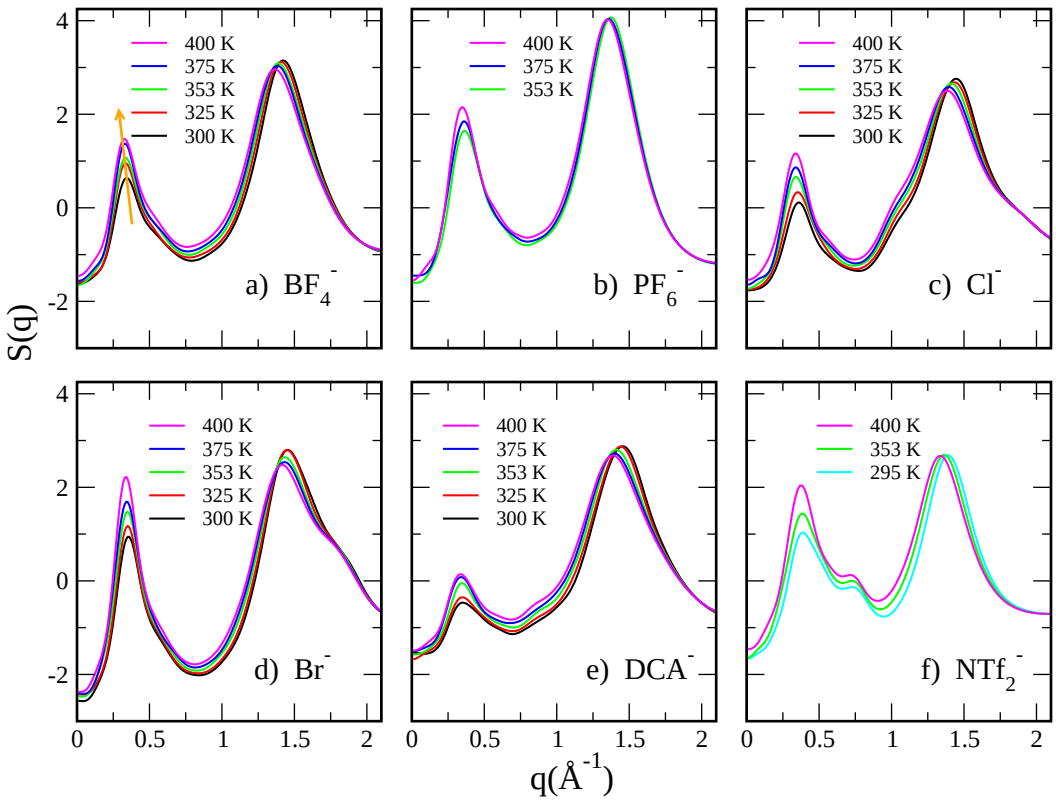

Figure 5.7: Temperature-dependence of the total S(q) for (a) $P_{14,6,6,6}{}^{+}/BF_4^-$ (b) $P_{14,6,6,6}{}^{+}/PF_6^-$ (c) $P_{14,6,6,6}{}^{+}/Cl^-$ (d) $P_{14,6,6,6}{}^{+}/Br^-$ (e) $P_{14,6,6,6}{}^{+}/DCA^-$ and (f) $P_{14,6,6,6}{}^{+}/NTf_2^-$ ILs. In all cases an increase in temperature results in a prepeak intensity increase. Notice that an intensity increase is also observed in the charge alternation region but not on adjacency correlations.

$$S^{Polar-Polar}(q) = S^{c_{Head}-c_{Head}}(q) + S^{a-a}(q) + S^{c_{Head}-a}(q) + S^{a-c_{Head}}(q),$$

$$S^{Apolar-Apolar}(q) = S^{c_{Tail}-c_{Tail}}(q),$$

$$S^{Polar-Apolar}(q) + S^{Apolar-Polar}(q) = S^{c_{Head}-c_{Tail}}(q) + S^{c_{Tail}-c_{Head}}(q) + S^{c_{Tail}-a}(q) + S^{a-c_{Tail}}(q).$$

In these equations the definition of 'head' and 'tail' refers to atoms in Fig. 5.1.

Interestingly, the purely apolar contribution to the prepeak diminishes with increasing temperature as is shown in Fig. 5.8. In other words, this subcomponent follows the intuitive behavior where an increase in temperature negatively impacts periodicity. As shown in Fig. 5.8 this behavior is generic for all systems studied. Instead, the purely polar contribution to the prepeak increases with increasing temperature which is counter intuitive. The behavior of cross polar-apolar correlations is complex, but in most cases an increase in temperature results in loss of polar-apolar correlation which because of its antipeak nature increases overall prepeak intensity.

In simple terms, the polar subcomponent is more correlated or periodic at higher temperatures but the apolar subcomponent is less periodic. The cross correlation between polar and apolar subcomponents appears to be less periodic as well.

Whereas we do not have a definitive explanation for this phenomenon, we can connect these observations with ideas we recently introduced in a set of articles[102, 110]. In these, we proposed that ionic liquids can be described as composed of frictionally stiff (high electrostriction) and frictionally soft (charge depleted) regions. Stiff and soft regions are associated with distinct local friction, high friction in the charge enhanced region and low friction in the charge depleted region. We notice in the current study that upon an increase in temperature, dispersion energy terms are negatively impacted to a much larger extent than Coulomb interactions.

In fact, the value of these changes are remarkably similar across liquids (see table T.1) even when total energy values may not be. This hints at a similar

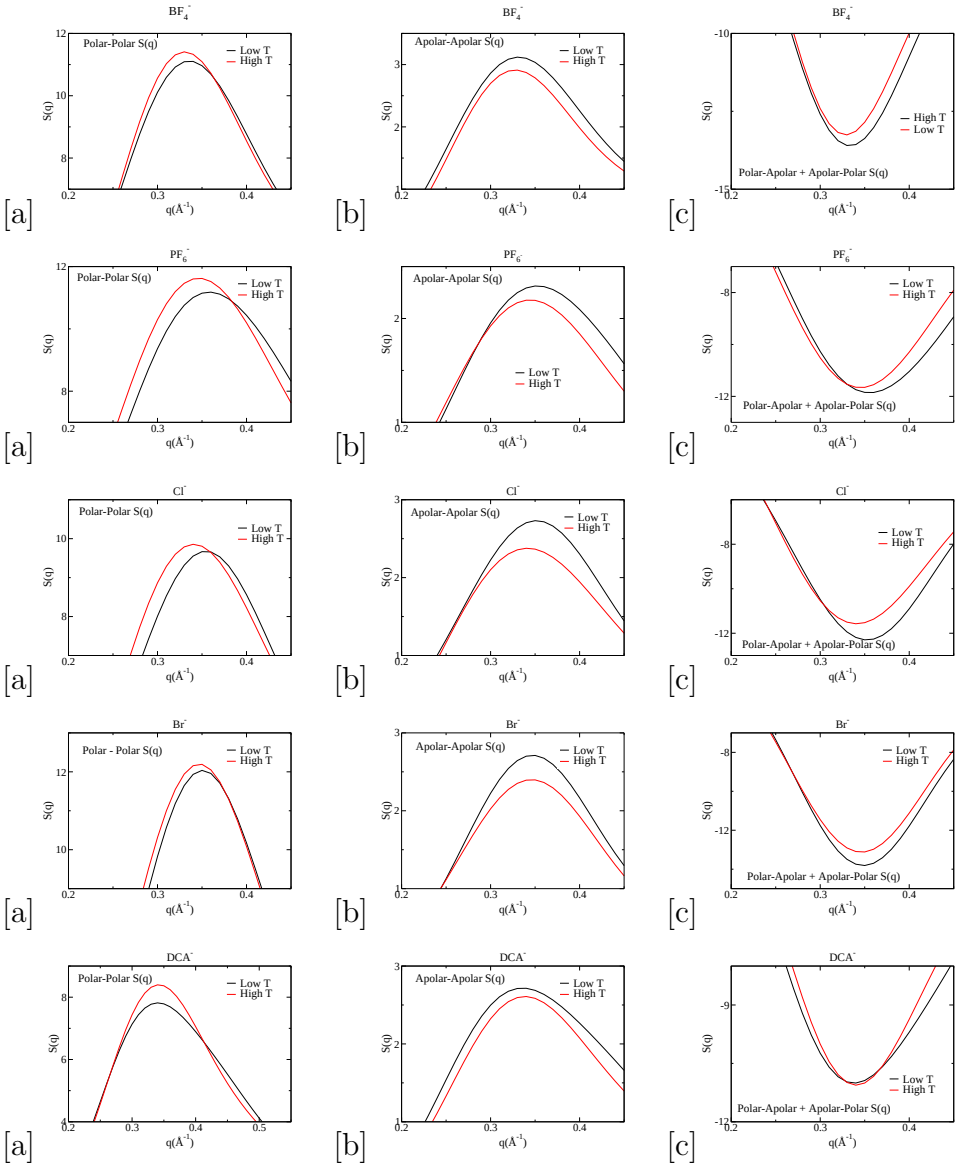

Figure 5.8: Temperature dependence of the polar-polar, apolar-apolar and polar-apolar + apolar-polar partial subcomponents of S(q) at q values consistent with the first sharp diffraction peak for the $P_{14,6,6,6}{}^{+}$ILs at 353 K and 300 K. In all cases the volume expansion caused by a temperature increase results in peaks and antipeaks shifting to lower q values.

Table 5.1: The Effect of Temperature on Coulomb and Lennard-Jones Energies.

IL	Energy(kJ/ mol)	Low T	High T	E_{HighT} - E_{LowT}
$P_{14,6,6,6}{}^{+}/BF_4^-$	$E_{Coulomb}$	-261672.3	-258718.0	2954.3
	$E_{Lennard\ Jones}$	-162372.6	-147748.9	14623.7
$P_{14,6,6,6}{}^{+}/PF_6^-$	$E_{Coulomb}$	-239818.7	-236964.9	2853.8
	$E_{Lennard\ Jones}$	-170883.3	-156489.3	14394.0
$P_{14,6,6,6}{}^{+}/Cl^-$	$E_{Coulomb}$	-313075.8	-310084.9	2990.9
	$E_{Lennard\ Jones}$	-148091.8	-134643.5	13448.27
$P_{14,6,6,6}{}^{+}/Br^-$	$E_{Coulomb}$	-300626.5	-297755.4	2871.1
	$E_{Lennard\ Jones}$	-149251.1	-135725.3	13525.8
$P_{14,6,6,6}{}^{+}/DCA^-$	$E_{Coulomb}$	-267643.0	-263924.7	3718.3
	$E_{Lennard\ Jones}$	-180087.8	-164796.8	15291.0
$P_{14,6,6,6}{}^{+}/NTf_2^-$	$E_{Coulomb}$	-17727.8	-14358.7	3369.1
	$E_{Lennard\ Jones}$	-219237.8	-201578.0	17659.8

fluidization[111, 112, 113, 114, 115] of the "soft" apolar regions in all $P_{14,6,6,6}{}^{+}$ containing systems upon a temperature increase and corresponding volume expansion of the liquid.

In contrast not much happens to the stiff liquid subcomponent (the charge network) except that it has to exist in a slightly larger volume. Charge alternation and polarity alternation occur at different wavenumbers but are not structurally decoupled. Better defined local charge ordering may imply better defined charge networks that contribute to an increase in prepeak intensity. To expand on this concept, notice that in our systems prepeaks of higher intensity occur concomitant with intensity increases in the charge alternation region (see S(q) at values in the range q≈ 0.7-1.1Å^{-1} in Fig. 5.7). It would appear that charge alternation associated with the first solvation shell is better organized at higher temperature and larger volume. To

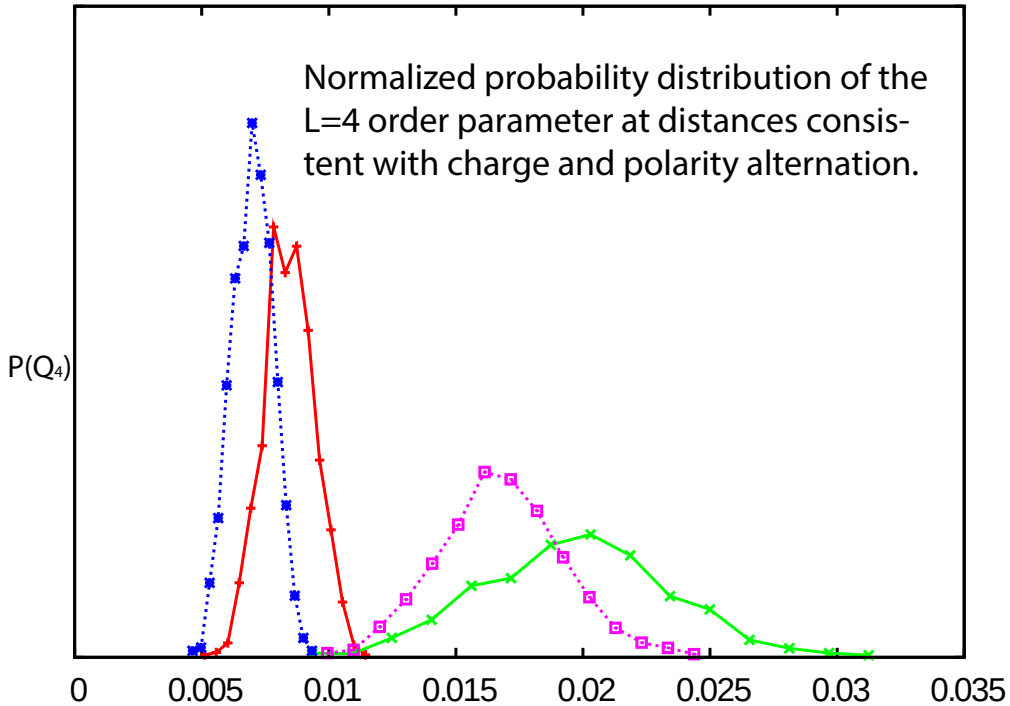

Figure 5.9: For the system $P_{14,6,6,6}{}^{+}/BF_4^-$, dashed blue and solid red lines correspond to the order parameter Q_4 for low (300 K) and high (400 K) temperatures in the case of the polarity alternation region. Dashed magenta and solid green lines correspond to the order parameter Q_4 for low (300 K) and high (400 K) temperatures in the case of the charge alternation region.

further confirm this, in Fig. 5.9 we present the probability distribution of the fourth spherical harmonic which has been used in the past[116] as an order parameter to describe orientational order in condensed phase systems. It is clear from Fig.5.9 that this parameter is enhanced both at charge alternation distances but also at distances consistent with the polarity alternation prepeak. This suggests that the fluidization of the apolar subcomponent and volume expansion in $P_{14,6,6,6}{}^{+}$ based liquids results in more defined local charge order that propagates through the percolating polar network to the nanoscale regime. In other words, a temperature increase results in a better defined polar network and consequently in a higher first sharp diffraction peak intensity.

CHAPTER 6
BICONTINUITY AND MULTIPLE LENGTH SCALE ORDERING IN PROTIC AND FLUOROPROTIC IONIC LIQUIDS.

6.1 Introduction

Recently novel and exciting design ideas have emerged that challenge our current understanding of IL morphology. In some cases these involve ILs with polar tails; we call these systems monophilic as opposed to the proverbial case of polar heads and apolar tails which are normally called biphilic. An example of these systems are ILs containing tail ether functionalities.[117, 101, 118] Other very recent developments are the so-called triphilic ILs in which polar groups, apolar alkyl tails and significantly large fluorinated tails are present. Pioneering experimental studies by the groups of Yoshida,[119] Triolo[81], Rebelo and Canongia Lopes[120] as well as work from the group of Drummond[121] lead us to believe that there possibly is a very interesting interplay between components with different polarity in these liquids and that this combined with hydrogen bonding can lead to new and exciting topological arrangements of ions as recently proposed for protic ILs.[122, 123, 124, 125, 126, 127, 128] However, a full mathematical and computational description of the sub-ionic components of $S(q)$ is still missing, and hypotheses about the origin of the different peaks in $S(q)$ for these types of systems are yet to be fully explored.

This chapter focuses on the computational description of the triphilic buty-

---

*Portion of this chapter is reproduced from The Journal of Physical Chemistry B. vol. 118, page 1270612716, year 2014 by J.J. Hettige, J.C. Araque, and C.J. Margulis. Copyright - Appendix C. DOI: 10.1021/jp5068457

lammonium pentadecafluoro-octanoate (BAOF) IL as compared to its non-fluorinated analog butylammonium octanoate (BAO) shown in fig. 6.1,

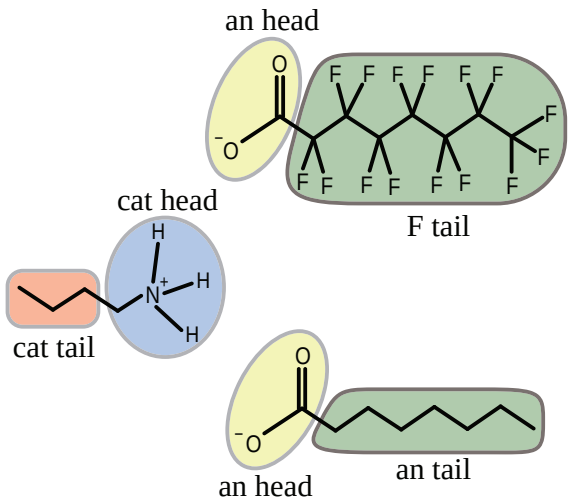

Figure 6.1: Scheme showing the definition of group partitions of the structure function $S(q)$ that are used throughout this chapter in the case of BA (left), OF (upper right) and O (lower right).

that the Drummond group has synthesized and studied via small- and wide-angle X-ray scattering (SWAXS). [121] In this study we go beyond what so far our group has been able to accomplish in terms of analyzing $S(q)$. We will show that both of these systems are continuously percolated by charge alternation strings or filaments that bifurcate creating disordered bicontinuous phases and that peaks in $S(q)$ can either be associated with inter-filament characteristic distances (the prepeak)

or intra-filament repeating patterns (peaks at larger q values).

6.2 Results and Discussion

Drummond and coworkers performed SWAXS experiments on a set of amonnium based and pyrrolidinium based ILs coupled with fluorinated carboxylate anions. [121] Of particular interest are studies that couple the BA cation with the OF anion because these ions incorporate a cationic alkyl tail and a significantly long anionic fluorinated tail. Furthermore this fluoroprotic IL can be compared with its non fluorinated analog BAO. Interestingly, Drummond and coworkers found that SWAXS intensity profiles show three peaks at about 0.33 Å^{-1}, 0.63 Å^{-1} and 1.22 Å^{-1} in the case of BAOF but only two peaks at around 0.36 $\text{Å}^{-1}$and 1.45 Å^{-1} in the case of BAO. Their interpretation of the three peaks in the case of BAOF was based on the assumption of fluorinated and hydrocarbon domains that each are segregated accounting for the two peaks with lowest q value and cation tail-cation tail adjacency correlations accounting for the peak at higher q value. In the case of BAO the absence of one of the three peaks was interpreted as an indication that only one type of hydrophobic domain (and not two as in the case of BAOF) was associated with the long anionic alkyl tails.[121]

Figures 6.2 a) and 6.2 b) show our computationally derived structure functions for BAOF and BAO respectively. Insets include the $I_{coh}(q)$ for comparison with the results of Drummond and coworkers (see Fig. 11 in reference [121]). In close agreement with experimental results our $I_{coh}(q)$ also show two peaks in the case of

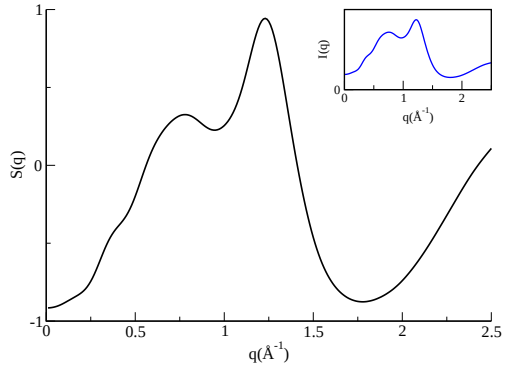

[a]

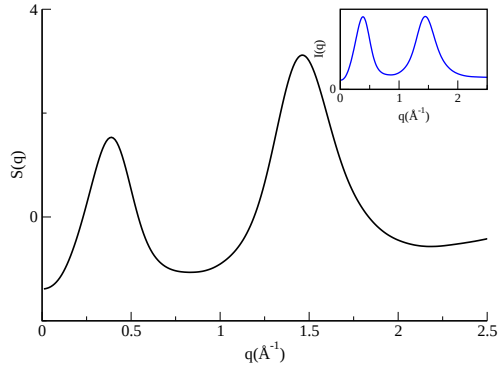

[b]

Figure 6.2: The total structure function $S(q)$ and coherent intensities $I_{coh}(q)$ (inset) for (a) BAOF and (b) BAO.

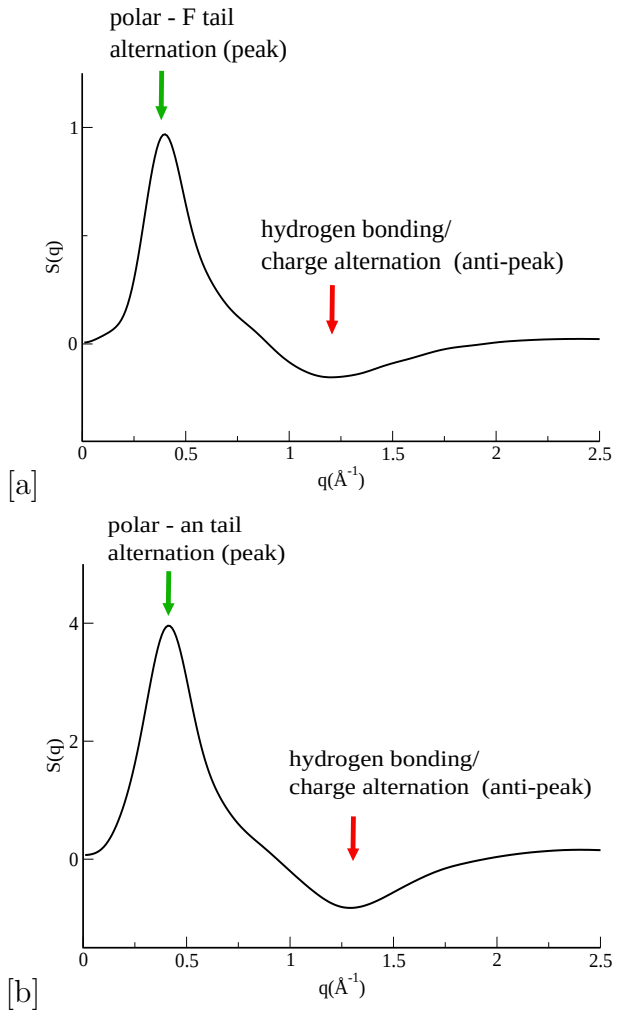

Figure 6.3: Cation head-anion head partial subcomponent of $S(q)$ for (a) BAOF and (b) BAO.

BAO and three peaks in the case of BAOF approximately at the correct wave number. Having established that our computational model is accurate to reproduce the overall $S(q)$ and $I_{coh}(q)$, we proceed to analyze in detail the physical origin of the different scattering features.

To better dissect and understand liquid morphology, in fig. 6.1 we define and label groups of atoms for which partial contributions to the overall $S(q)$ will be emphasized throughout this chapter.

6.2.1 The Defining Property of Both ILs is a Hydrogen Bonding Charge Alternation Network that Percolates them Resulting in Bicontinuous Phases.

We seek first to understand charge and polarity alternation. We recall from prior work[100, 99] that the polar cationic-polar anionic partial subcomponent of $S(q)$ defined as $S^{cat_{head}-an_{head}}(q) + S^{an_{head}-cat_{head}}(q)$ is the most natural mathematical function to investigate the distinct q ranges where polarity and charge alternation in ILs manifest.[99] The reader is encouraged to read reference [99] for a thorough explanation of why this is the case, but briefly it can be shown that in the range of q values where charge alternation occurs this function is expected to have a negative going peak (commonly called antipeak) and in the range of q values where polarity alternation occurs this same function is expected to have a positive going peak (the prepeak or first sharp diffraction peak).

Figures 6.3 a) and 6.3 b) show the polar cationic-polar anionic partial subcomponent of $S(q)$ in the cases of BAOF and BAO respectively. Vertical arrows indicate

the q values at which polarity alternation (smaller q peak) and charge alternation (larger q peak) occur. We will show in subsequent subsections that the polarity alternation peak in figures 6.3 a) and 6.3 b) correspond mainly to the separation between hydrogen-bonded filaments that percolate the whole liquid. These filaments are separated by alkyl and fluorocarbon spacer chains in the case of BAOF and by short and long alkyl tails in the case of BAO. Instead in this subsection we focus only on the charge alternation antipeak that occurs within single filaments and is reflected at q values around 1.15-1.3 Å^{-1}.

Figure 6.6 shows a typical example in which the analysis described in section 1.5 is used to identify important contributions to the charge alternation region q_{ch-alt} that are at distance about $2\pi/q_{ch-alt}$. We see that two cations and two anions form a hydrogen bonded ring that allows for second hydrogen bonded connections to the second carboxylate oxygens of each of the partner anions. Further connections are also possible at other proton locations of ammonium nitrogen. On average in the case of BAOF there are close to three hydrogen bonds per cation head and about 3.5 oxygen atoms in the first solvation shell. This is shown in Figures 6.4 and 6.5 where the number of hydrogen bonds as a function of time and the integral of the N-O $g(r)$ are plotted respectively. What is shown in fig. 6.6 is just an example of a "hydrogen bonding unit" and many variations of this structure are indeed found by inspection and careful mathematical analysis of the polar subcomponent of $S(q)$.

Whereas fig. 6.6 shows a particular hydrogen bonding unit, such units are part of a complex network made of one dimensional filaments shown in Fig. 6.7 a) and 6.7

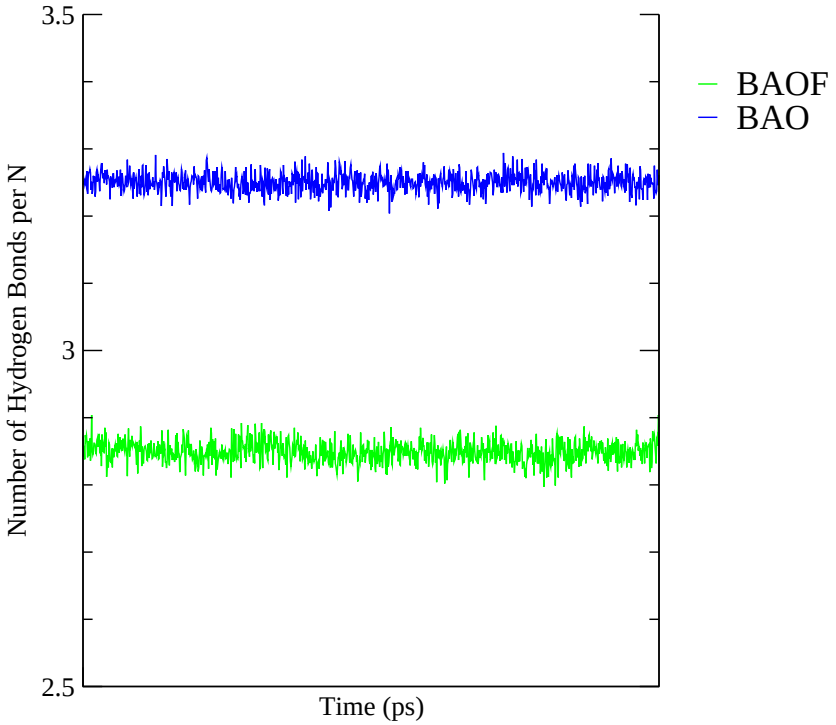

Figure 6.4: Number of hydrogen bonds per N atom in BAOF and BAO as a function of time. The X-axis covers a time duration of 1 ns.

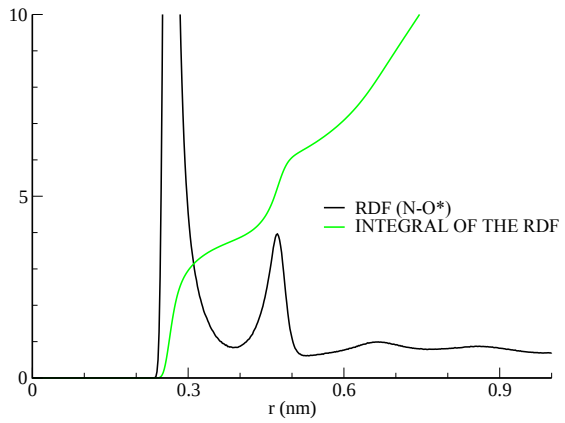

[a]

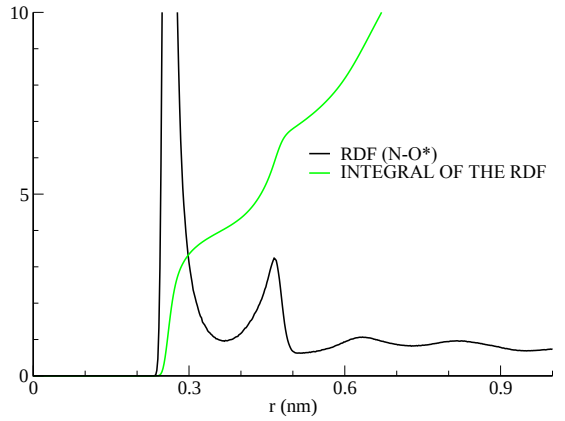

[b]

Figure 6.5: Radial distribution function (RDF) and its integral for N and all O atoms in the case of (a) BAOF and (b) BAO.

b) . A closer look of such hydrogen bond network is shown in fig. 6.8. We will refer to this figure repeatedly because it clearly conveys all of the main features present in BAOF, namely hydrogen bonding charge alternation, the typical separation between filaments giving rise to the prepeak and the apolar-fluorinated alternation within single filaments that contributes significantly to the intermediate peak in $S(q)$.

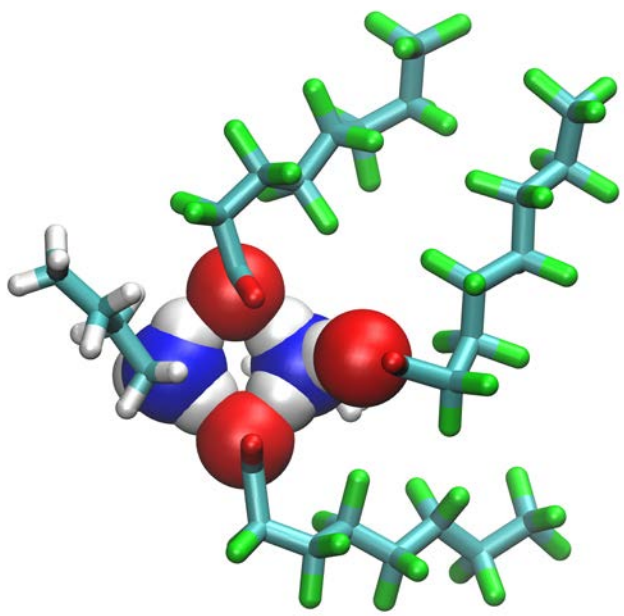

Figure 6.6: A hydrogen bonding unit observed in BAOF, red corresponds to anion O, and dark blue to cation N.

In terms of hydrogen bonding and charge alternation, the case of BAO is not too different from what we see for BAOF. Figure 6.3 b) is certainly very similar to fig. 6.3 a) and analysis of $S(q)$ to look for important contributors to charge alternation

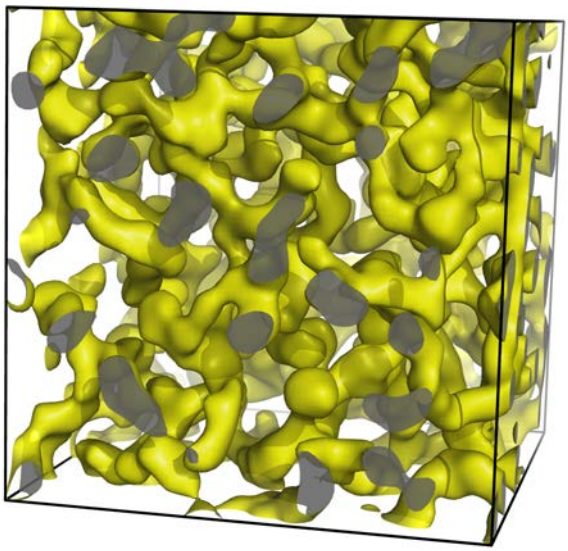

[a]

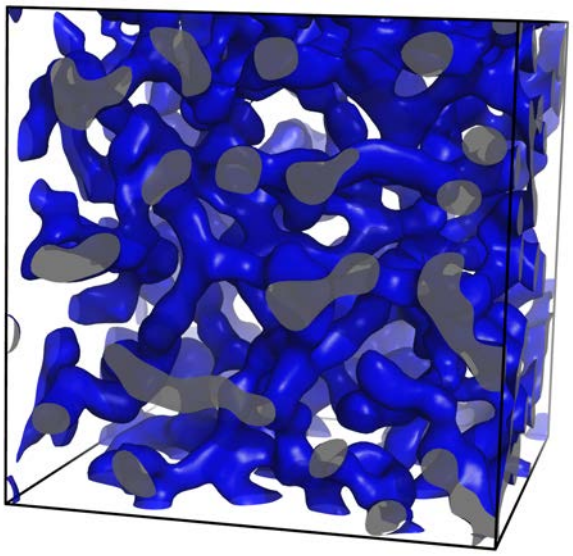

[b]

Figure 6.7: Isosurfaces representing the sub-volume occupied by the hydrogen bond network as defined in reference [9] for the case of (a) BAOF and (b) BAO.

results in very similar patterns to those derived for BAOF.

Interestingly, because of the geometries in which these hydrogen bond interactions occur, the charge alternation antipeak appears at significantly larger q values (shorter real space distance) than commonly observed in other ILs. Normally adjacency correlations occur as a broad peak at around 1.5 Å^{-1}, whereas charge alternation occurs at or somewhat below 1 Å^{-1}. In the case of BAOF and BAO charge alternation occurs at around 1.15 and 1.3 Å^{-1} respectively, overlapping to some extent with the q range in which adjacency correlations of different nature appear in S(q) as properly interpreted by Drummond and coworkers.[121] Because in these protic systems charge alternation occurs at shorter distance, it is expected that the antipeak in fig. 6.3 will be broader. This is in part because a given range of distances corresponds to a much larger range of q values when q is large.

6.2.2 The Molecular Origin of the First Sharp Diffraction Peak

Both for BAO and BAOF experimental and computational $I(q)$ show prominent prepeaks at around 0.36-0.4 Å^{-1}. If this peak is the result of some type of polarity alternation (in the case of BAOF polar-fluorocarbon alternation and in the case of BAO polar-alkyl tail alternation) there should be clear signature of this in the subcomponents of $S(q)$.[55, 56] At $q_{prepeak}$, in the case of BAOF, one can expect a peak both in the polar-polar subcomponent of $S(q)$ ($S^{cat_{head}-cat_{head}}(q) + S^{an_{head}-an_{head}}(q) + S^{cat_{head}-an_{head}}(q) + S^{an_{head}-cat_{head}}(q)$) as well as in the fluorocarbon-fluorocarbon subcomponent of $S(q)$ ($S^{Ftail-Ftail}(q)$). At $q_{prepeak}$ the polar-fluorocarbon subcomponent

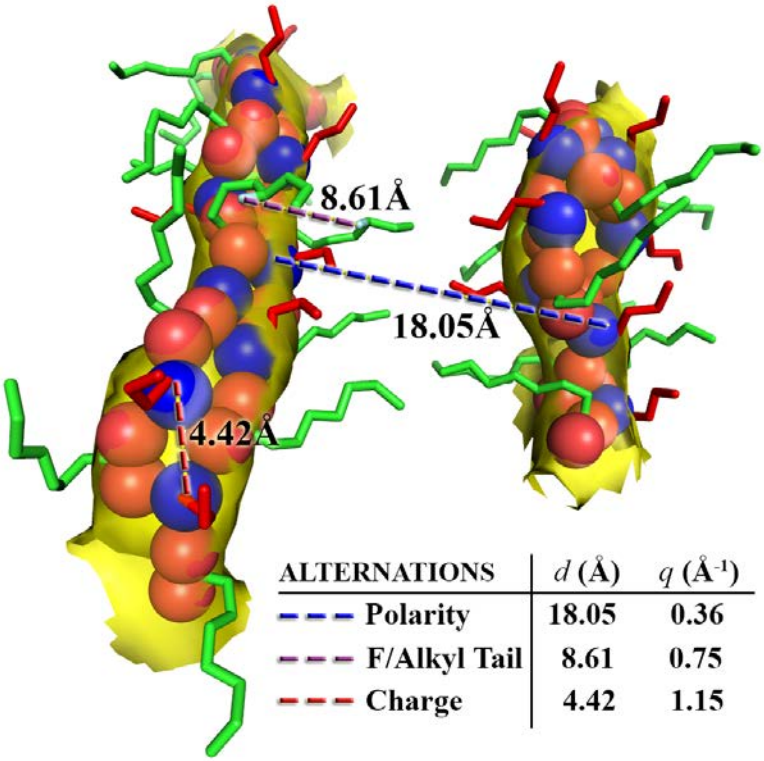

Figure 6.8: Typical structure of hydrogen-bonded filaments in the case of BAOF. In this depiction we see all three structural features that define this liquid, namely hydrogen-bonded charge alternation (highlighted with a dashed line is the typical nitrogen-nitrogen separation distance), fluorinated tail-alkyl tail alternation (highlighted with a dashed line on the left filament) and the typical separation between filaments in the network (highlighted with a dashed line connecting two different filaments). The blue and red spheres represent the van der Waals volume of the nitrogen and oxygen atoms in the cation and anion head, respectively. The red and green sticks represent the configuration of cationic and anionic tails, respectively. The yellow iso-surface is as described in fig. 6.7.

$(S^{cat_{head}-Ftail}(q)+S^{Ftail-cat_{head}}(q)+S^{an_{head}-Ftail}(q)+S^{Ftail-an_{head}})$ should instead show an antipeak.[55, 56] Figure 6.9 a) clearly confirms this prediction. A similar situation can be observed in the case of BAO (see Figure 6.9 b) One should simply conclude that in the case of BAOF (fig. 6.9 a) the first sharp diffraction peak is a result of polar-fluorocarbon alternation and in the case of BAO (Figure 6.9 b) it is a result of alternation between polar groups and anion alkyl tails.

A typical ionic arrangement giving rise to the prepeak in the case of BAOF is displayed in fig. 6.10. This structure was not extracted from visual inspection of the simulation box but instead via the protocol described in section 1.5. Such structure corresponds to two distinct polar groups at distance $2\pi/q_{prepeak}$ separated by fluorocarbon tails that strongly contribute to the prepeak intensity. To better understand the role of this common liquid motif in the context of the whole liquid the reader should envision each polar end in fig. 6.10 as forming part of a hydrogen bond filament and the fluorinated tails as filling the space in between. The filaments are shown in fig. 6.7 and the pattern of filaments separated by fluorocarbon are as shown in fig. 6.8

In fig. 6.7, the empty space is filled with fluorocarbon and alkyl chains. However, it is the separation between hydrogen bond filaments defined mostly by the length between opposing fluorocarbon tails that gives rise to the prepeak. The case of BAO is not too different from that of BAOF. The prepeak in this case corresponds to the distance between hydrogen bonded filaments separated by anionic hydrocarbon tails. Figure 6.9 a) shows an example of such common liquid pattern in the case of

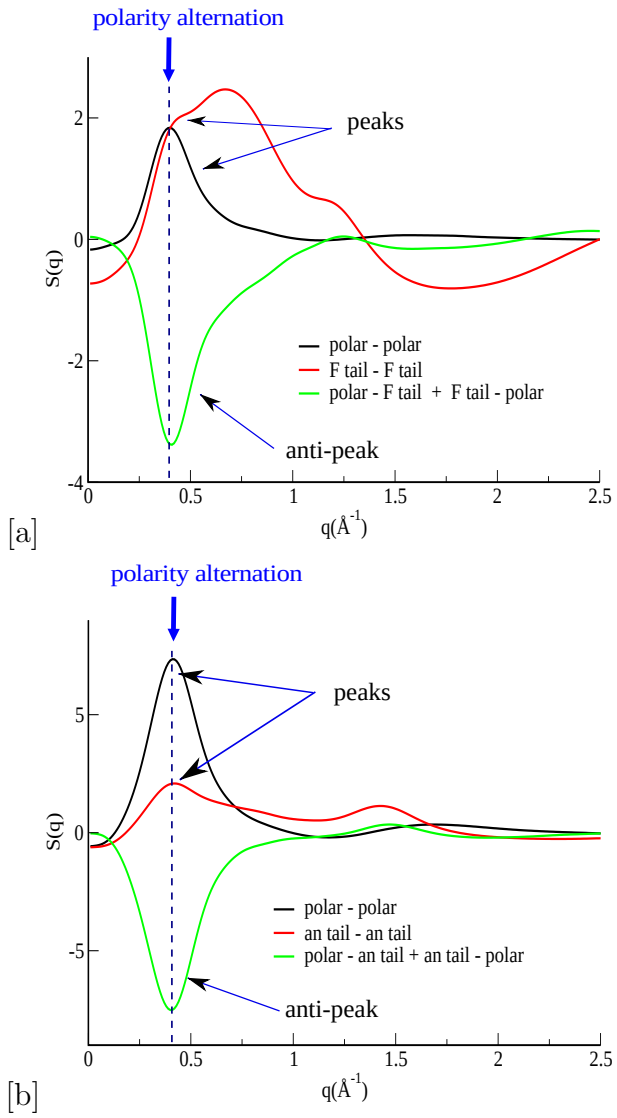

Figure 6.9: Polar-polar, polar-anion tail and anion tail-anion tail subcomponents of $S(q)$ for the case of (a) BAOF and (b) BAO. A vertical line in each figure indicates the q value at which polarity alternation occurs which should be interpreted in the context of fig. 6.10 as well as fig. 6.8.

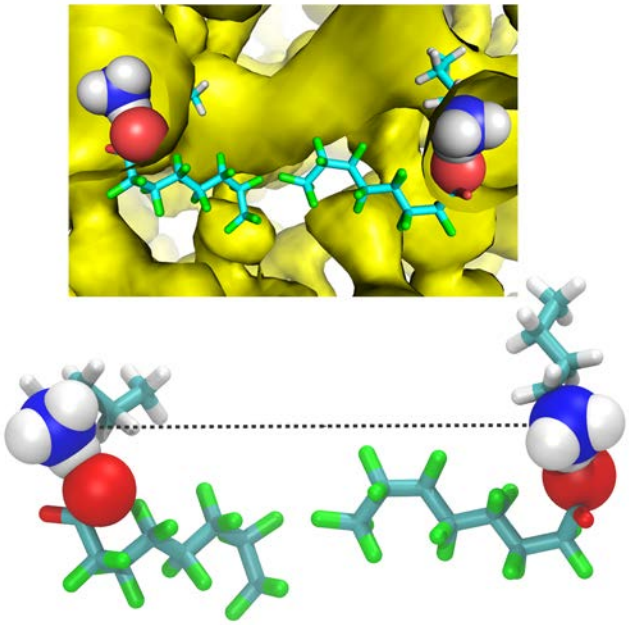

Figure 6.10: A realistic molecular level view of the polar-F tail alternation in BAOF. Green corresponds to fluorine atoms and white to hydrogen atoms, light blue to carbon atoms, red to oxygen atoms and dark blue to nitrogen atoms.

BAOF and fig. 6.9 b) shows the same pattern in the case of BAO.

In brief, both in the case of BAOF and BAO the prepeak is due to polar-anion tail alternations. The liquid landscape is dominated by a network of hydrogen bonds and the typical separation between hydrogen bond filaments is associated with the prepeak length scale. It is important to notice however that there are many other flourinated tail correlations in the case of BAOF as well as alkyl anion tail correlations in the case of BAO that are also consistent with the prepeak wave vector. Such correlations certainly contribute to the tail-tail subcomponents of $S(q)$ in both liquids making assignment of each peak to a single liquid feature inappropriate.

6.2.3 The Intermediate $S(q)$ Peak in BAOF

Figure 6.2 shows a peak at around 0.75 Å^{-1} in the case of BAOF that is absent in the case of BAO. The presence of a peak in one case and the absence in the other was originally assigned by Drummond and coworkers[121] to some type of aggregation of cationic alkyl tails in the case of BAOF that is absent in the case of BAO.

Our analysis of $S(q)$ described in section 1.5 provides a clear explanation for the origin of the $q_{intermediate}$ peak. Because of the charge alternating nature of the hydrogen bond filaments, cationic tails and anionic tails must naturally alternate. Another way of expressing this is that both cationic and anionic tails often point in directions perpendicular to the hydrogen bond filaments and therefore alkyl and fluorinated tails alternate in sync with the charges on the network. One can get an

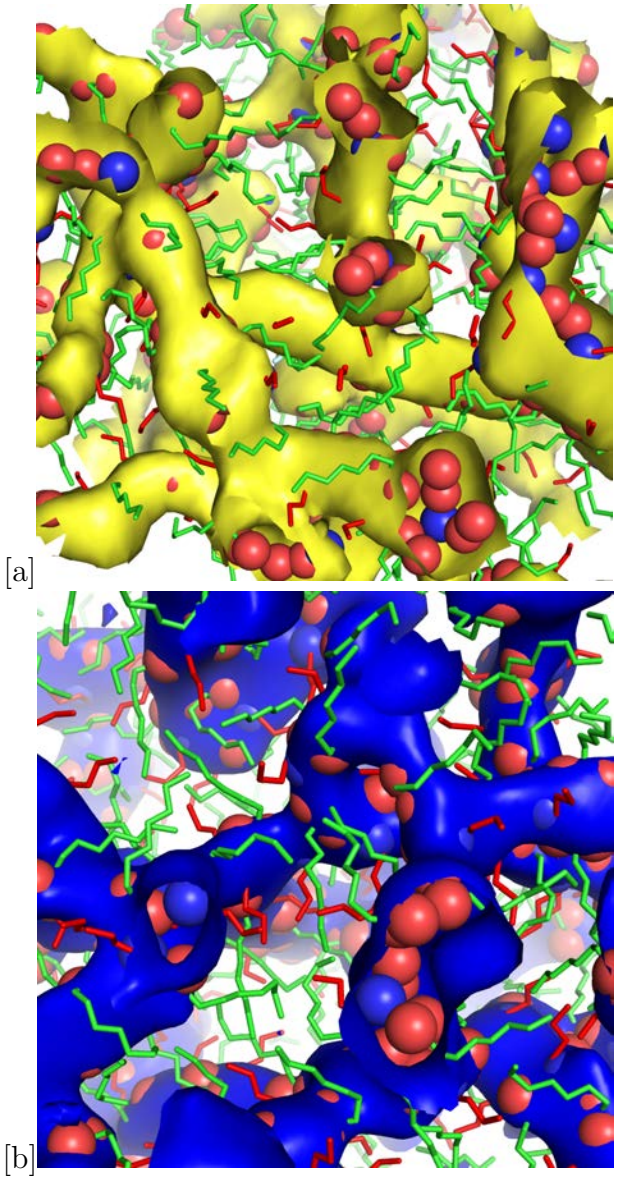

Figure 6.11: (a) Anionic fluorocarbon tails (green) and cationic alkyl tails (red) continuously percolated by a charge alternating hydrogen bond network (yellow) in the case of BAOF (b) Anionic alkyl tails (green) and cationic alkyl tails (red) continuously percolated by a charge alternating hydrogen bonded network (dark blue) in the case of BAO. In both subfigures the van der Waals volume of oxygen and nitrogen atoms in the network is depicted in red and blue respectively.

idea of what such an alternation looks like from fig. 6.12.

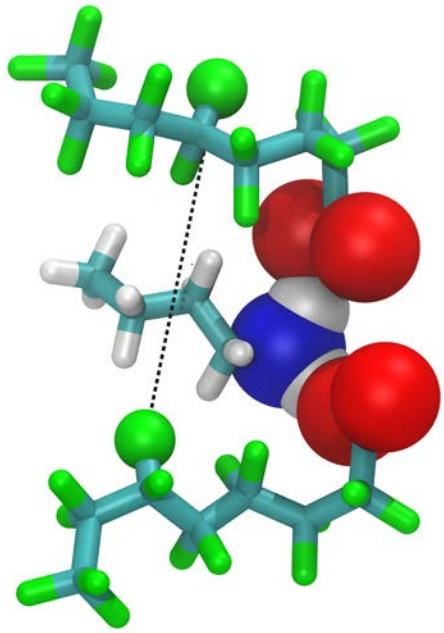

Figure 6.12: An important component contributing to the intermediate peak at about 0.75Å^{-1} in the case of BAOF where we can observe cation alkyl tail- anion fluorinated tail alternation. This pattern was chosen because it was deemed important at this q value from the analysis described in section 1.5. This alternation should be interpreted in the context of figures 6.14 and 6.15.

The fact that there is an alternation in BAOF at $q_{intermediate}$ can be gleaned from fig. 6.11 a) where the typical pattern of two peaks and one antipeak is highlighted. A peak at $q_{intermediate}$ appears in the F tail-F tail subcomponent of $S(q)$, another peak in the cation tail-cation tail subcomponents of $S(q)$. These are natu-

rally matched by an antipeak in the F tail-cation tail subcomponent of $S(q)$ at the same q value. That this is the signature of F tail-cation tail alternation can be understood from derivations and arguments in references [55] and [56]. Whereas cationic alkyl tail-anionic F tail alternation is not the only contribution responsible for the large F tail-F tail subcomponent of $S(q_{intermediate})$ it certainly is an important one.

How does the alternation shown in fig. 6.12 fit within the context of the liquid? Are fluorinated tails and alkyl tails segregated? We can begin understanding this by considering fig. 6.14. We see that charge alternating hydrogen bond filaments are decorated by anionic fluorinated tails and cationic alkyl tails that each form strips (green in the case of the F tails and red in the case of the alkyl tails). Within a single hydrogen bond filament, red and green decorating strips alternate and tend not to mix. The alternation between these strips gives rise to individual ionic correlations such as that shown in fig. 6.12.

Interestingly the case of BAO is strikingly similar (see fig. 6.15) and the reason why a peak is not seen in the overall $S(q)$ at $q_{intermediate}$ is because of perfect cancellations. This can be verified from the pattern of peaks and antipeaks in fig. 6.11 b) In the case of BAO the two peaks and the antipeak contributing to cationic tail-anionic tail alternation simply add up to an overall flat $S(q_{intermediate})$. This phenomenon of perfect cancellation of alternations is certainly not uncommon.[1]

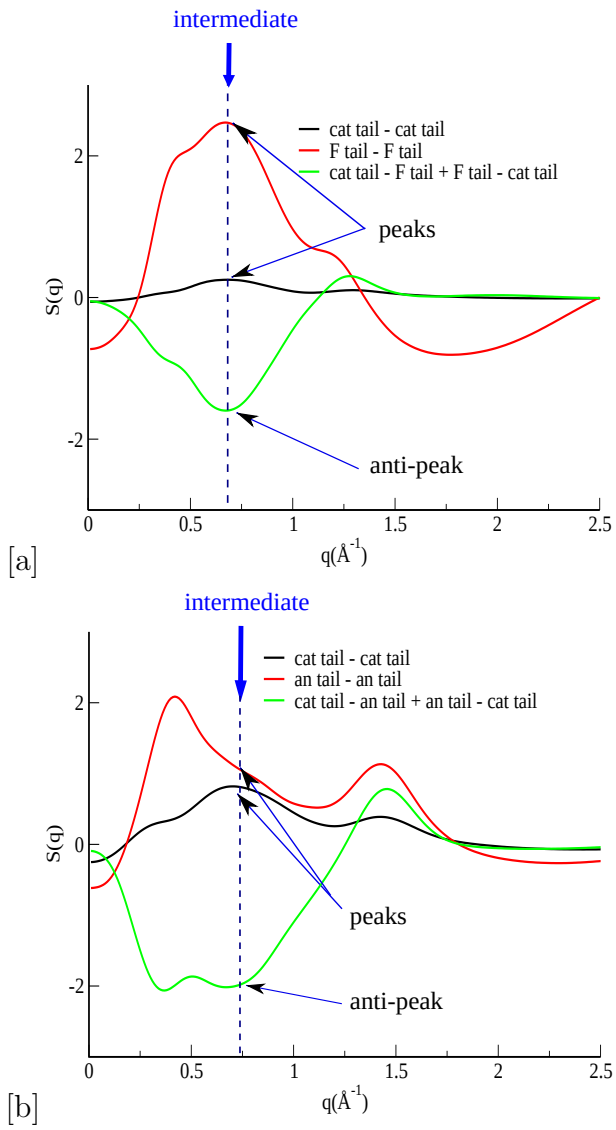

Figure 6.13: Cation tail-cation tail, anion tail-anion tail and cation tail-anion tail subcomponents of $S(q)$ in the case of (a) BAOF and (b) BAO. A vertical dashed line indicates the q value at which long anionic and short cationic tail alternation occurs. This alternation should be understood in the context of fig. 6.14 and fig. 6.15.

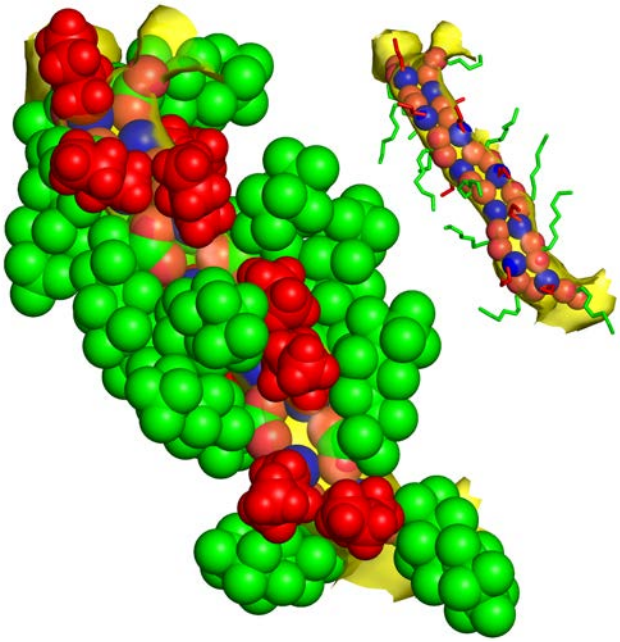

Figure 6.14: The context within single filaments in which the anionic fluorinated tails (green) and cationic alkyl tails (red) alternate and give rise to the peak at 0.75Å^{-1} in $S(q)$ in the case of BAOF.

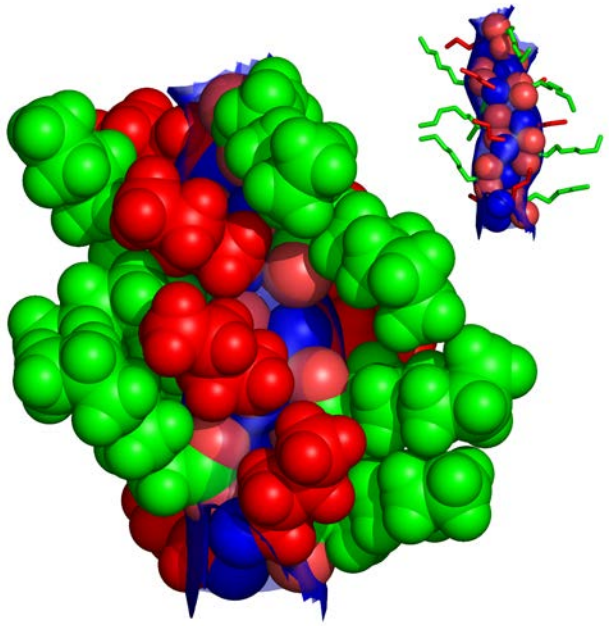

Figure 6.15: The context within single filaments in which the long anionic alkyl tails (green) and short cationic alkyl tails (red) alternate in the case of BAO.

6.3 Conclusions: An Emerging Picture of the Liquid Landscape

Both in the case of BAOF and BAO, the emerging picture arising from this study is that of multiscale ordering that encompasses from the atomic to the fully macroscopic. The main liquid feature is a fully connected percolating network of charge alternating hydrogen bonds that renders these systems bicontinuous. The distance between hydrogen bond filaments gives rise to the prepeak. Because the long anionic tails define the separation between filaments they also define the q value at which the prepeak occurs. Filaments in the hydrogen bond network are decorated by strips of long anionic tails and short cationic tails that alternate. In the case of BAOF this alternation gives rise to intermediate range order via apolar-fluorinated segregation within the surface of each individual filament. In both liquids, long anionic and short cationic tails are anchored to the filaments by charged atoms. These charged atoms are capable of hydrogen bonding and their charge alternation defines the backbone of the filaments forming the network. Because in the case of BAOF fluorinated tails are bulkier than anionic alkyl tails in the case of BAO, certain differences exist in the liquid morphology that are reflected in $S(q)$. One example is the complete cancellation of the peak at $q_{intermediate}$ in the case of BAO that is present in the case of BAOF.

BAOF is one in a class of ILs that has been called triphilic. The name is well deserved in that the charge alternation imposes two phases bicontinuously intertwined, one purely made of charged alternating filaments and the other made of fluorinated and alkyl components. Within the non-charged subcomponent, fluorinated and alkyl

tails are also segregated by an arrangement imposed by charge alternation along filaments. The organization is in the form of strips that decorate the charged filaments, giving the liquid the desired three segregated component identity.

CHAPTER 7
SUMMARY, IMPACT AND FUTURE ENDEAVORS.

The objective of the work related to this dissertation has been to study the nanoscale structure of different ionic liquids using molecular dynamics simulations in the context of X-ray scattering experiments. A major concern unraveled by our studies is that signal cancellations at q values associated with alternations can completely hide important liquid features and result in wrong interpretation of experimental results. These missing features in the experimental S(q) are a consequence of the perfect cancellation between peaks and antipeaks observed in its partial subcomponents. We have proposed that the cation head-anion partial subcomponent of S(q) derived from simulations can unambiguously reveal such length scales associated with alternations in the liquid phase.

Another finding of these studies highlights that even though cations are often more structurally rich and may significantly define the liquid landscape, in terms of X-ray scattering experiments, anions act as major reporters of structure. This is because anions often have the largest X-ray form factors.

The temperature dependent study carried out on six phosphonium ionic liquids shows an anomalous dependence of the prepeak intensity on temperature. It would appear from our studies that in phosphonium ionic liquids at higher temperature, the polar groups are more organized at the expense of a fluidization of apolar alkyl tails. Instead, at lower temperature, the apolar groups are more organized at the expense of polar groups. The prepeak intensity is a result of both these effects that are opposite

in nature. Since the anions are often important reporters of structure, the increase in polar-polar correlations at higher temperature heavily impact X-ray intensities. The increase in prepeak intensity is a consequence of the better defined polar network at higher temperature.

The structural study carried out on the fluoroprotic and nonfluoroprotic ionic liquids namely, butylammonium pentadecafluoro-octanoate and butylammonium octanoate, reveals that the main liquid feature is a continuous hydrogen bond percolating network. This hydrogen bonded network is decorated by anionic and cationic tails that alternate. The segregation between the two components (one made of continuous filaments and the other made of fluorinated and/or alkyl tails) makes these ionic liquids bicontinuous. The structures of the fluorinated and non fluorinated systems look very similar while the missing intermediate peak (in the total S(q)) of the nonfluorinated ionic liquid is merely a consequence of the perfect cancelation of peaks and antipeaks.

This dissertation is based on the ionic liquids that are mostly amphiphilic. Departing from this paradigm, the inclusion of butylammonium pentadecafluoro-octanoate highlights that other design ideas could be very interesting. Our group has recently studied the case of liquids in which cationic tails are not apolar,[101] and I have recently started pursuing work on 1-methyl-3-octylimidazolium octylsulfate in comparison with 3-[2-(2-ethoxyethoxy)ethyl]-1-methylimidazolium 2-(2-ethoxyethoxy) ethylsulfate. In one case both the cation and anion have alkyl tails whereas in the other both have ether containing tails that render them much less apolar. We are

interested in the properties of these systems in the bulk as well as at interfaces. These systems depart from the typical polar/apolar rule that is a common motif of many ILs. How solutes will interact with such systems is not yet clear and should be studied in the future.

APPENDIX A
COPYRIGHTS

Copyright Clearance Center RightsLink®

Home | Create Account | Help | Live Cha

ACS Publications
Most Trusted. Most Cited. Most Read.

Title: Bicontinuity and Multiple Length Scale Ordering in Triphilic Hydrogen-Bonding Ionic Liquids

Author: Jeevapani J. Hettige, Juan Carlos Araque, Claudio J. Margulis

Publication: The Journal of Physical Chemistry B

Publisher: American Chemical Society

Date: Nov 1, 2014

Copyright © 2014, American Chemical Society

LOGIN

If you're a copyright.com user, you can login to RightsLink using your copyright.com credentials. Already a RightsLink user or want to learn more?

PERMISSION/LICENSE IS GRANTED FOR YOUR ORDER AT NO CHARGE

This type of permission/license, instead of the standard Terms & Conditions, is sent to you because no fee is being charged for your order. Please note the following:

- Permission is granted for your request in both print and electronic formats, and translations.
- If figures and/or tables were requested, they may be adapted or used in part.
- Please print this page for your records and send a copy of it to your publisher/graduate school.
- Appropriate credit for the requested material should be given as follows: "Reprinted (adapted) with permission from (COMPLETE REFERENCE CITATION). Copyright (YEAR) American Chemical Society." Insert appropriate information in place of the capitalized words.
- One-time permission is granted only for the use specified in your request. No additional uses are granted (such as derivative works or other editions). For any other uses, please submit a new request.

BACK | CLOSE WINDOW

Figure A.1: Copyright permission from The American Chemical Society for the article by J. J. Hettige, J. C. Araque, and C. J. Margulis, J. Phys. Chem. B 2014, 118, 12706-12716.

Copyright Clearance Center RightsLink®

Home | Create Account | Help | Live Chat

ACS Publications Most Trusted. Most Cited. Most Read.

Title: Modern Room Temperature Ionic Liquids, a Simple Guide to Understanding Their Structure and How It May Relate to Dynamics

Author: Juan C. Araque, Jeevapani J. Hettige, Claudio J. Margulis

Publication: The Journal of Physical Chemistry B

Publisher: American Chemical Society

Date: Oct 1, 2015

Copyright © 2015, American Chemical Society

LOGIN

If you're a copyright.com user, you can login to RightsLink using your copyright.com credentials. Already a RightsLink user or want to learn more?

PERMISSION/LICENSE IS GRANTED FOR YOUR ORDER AT NO CHARGE

This type of permission/license, instead of the standard Terms & Conditions, is sent to you because no fee is being charged for your order. Please note the following:

- Permission is granted for your request in both print and electronic formats, and translations.
- If figures and/or tables were requested, they may be adapted or used in part.
- Please print this page for your records and send a copy of it to your publisher/graduate school.
- Appropriate credit for the requested material should be given as follows: "Reprinted (adapted) with permission from (COMPLETE REFERENCE CITATION). Copyright (YEAR) American Chemical Society." Insert appropriate information in place of the capitalized words.
- One-time permission is granted only for the use specified in your request. No additional uses are granted (such as derivative works or other editions). For any other uses, please submit a new request.

BACK | CLOSE WINDOW

Figure A.2: Copyright permission from The American Chemical Society for the article by J. C. Araque, J.J. Hettige, and C. J. Margulis, J. Phys. Chem. B, 2015, 119 , 12727 -12740.

Copyright Clearance Center RightsLink®

Home | Create Account | Help | Live Chat

ACS Publications
Most Trusted. Most Cited. Most Read.

Title: Anions, the Reporters of Structure in Ionic Liquids
Author: Jeevapani J. Hettige, Hemant K. Kashyap, Harsha V. R. Annapureddy, et al
Publication: Journal of Physical Chemistry Letters
Publisher: American Chemical Society
Date: Jan 1, 2013
Copyright © 2013, American Chemical Society

LOGIN
If you're a copyright.com user, you can login to RightsLink using your copyright.com credentials. Already a RightsLink user or want to learn more?

PERMISSION/LICENSE IS GRANTED FOR YOUR ORDER AT NO CHARGE

This type of permission/license, instead of the standard Terms & Conditions, is sent to you because no fee is being charged for your order. Please note the following:

- Permission is granted for your request in both print and electronic formats, and translations.
- If figures and/or tables were requested, they may be adapted or used in part.
- Please print this page for your records and send a copy of it to your publisher/graduate school.
- Appropriate credit for the requested material should be given as follows: "Reprinted (adapted) with permission from (COMPLETE REFERENCE CITATION). Copyright (YEAR) American Chemical Society." Insert appropriate information in place of the capitalized words.
- One-time permission is granted only for the use specified in your request. No additional uses are granted (such as derivative works or other editions). For any other uses, please submit a new request.

BACK | CLOSE WINDOW

Figure A.3: Copyright permission from The American Chemical Society for the article by J.J. Hettige, H. K. Kashyap, H. V. R. Annapureddy, and C. J. Margulis, J. Phys. Chem. Lett., 2013, 4 , 105110.

Copyright Clearance Center RightsLink®

Home | Account Info | Help | Live Chat

Title: Communication: Anomalous temperature dependence of the intermediate range order in phosphonium ionic liquids

Author: Jeevapani J. Hettige,Hemant K. Kashyap,Claudio J. Margulis

Publication: Journal of Chemical Physics

Volume/Issue 140/11

Publisher: AIP Publishing LLC

Date: Mar 17, 2014

Page Count: 4

Rights managed by AIP Publishing LLC.

Logged in as:
Jeevapani Hettige
LOGOUT

Order Completed

Thank you very much for your order.

Click here for Payment Terms and Conditions.

Get a printable version for your records.

License Number	3738280034252
Order Date	Oct 29, 2015
Publisher	AIP Publishing LLC
Publication	Journal of Chemical Physics
Article Title	Communication: Anomalous temperature dependence of the intermediate range order in phosphonium ionic liquids
Author	Jeevapani J. Hettige,Hemant K. Kashyap,Claudio J. Margulis
Online Publication Date	Mar 17, 2014
Volume number	140
Issue number	11
Type of Use	Thesis/Dissertation
Requestor type	Author (original article)
Format	Electronic
Portion	Excerpt (> 800 words)
Will you be translating?	No
Title of your thesis / dissertation	Elucidating the Nanoscale Structure of Ionic Liquids via Molecular Dynamics Simulations
Expected completion date	Jan 2016
Estimated size (number of pages)	150
Total	0.00 USD

Figure A.4: Copyright permission from The American Institute of Physics for the article by J.J. Hettige, H. K. Kashyap, and C. J. Margulis, J. Chem. Phys. 2014, 140, 111102

REFERENCES

[1] Annapureddy, H. V. R.; Kashyap, H. K.; De Biase, P. M.; Margulis, C. J. *J. Phys. Chem. B* **2010**, *114*(50), 16838–16846.

[2] Santos, C. S.; Murthy, N. S.; Baker, G. A.; Castner, Jr., E. W. *J. Chem. Phys.* **2011**, *134*(12), 121101.

[3] Kilaru, P.; Baker, G. A.; Scovazzo, P. *J. Chem. Eng. Data* **2007**, *52*(6), 2306–2314.

[4] Manic, M. S.; Macedo, E. A.; Najdanovic-Visak, V. *Fluid Phase Equilib.* **2012**, *324*(0), 8 – 12.

[5] Diogo, J. C. F.; Caetano, F. J. P.; Fareleira, J. M. N. A.; Wakeham, W. A.; Afonso, C. A. M.; Marques, C. S. *J. Chem. Eng. Data.* **2012**, *57*(4), 1015–1025.

[6] Tariq, M.; Forte, P.; Gomes, M. C.; Lopes, J. C.; Rebelo, L. *J. Chem. Thermodyn.* **2009**, *41*(6), 790 – 798.

[7] Fraser, K. J.; Izgorodina, E. I.; Forsyth, M.; Scott, J. L.; MacFarlane, D. R. *Chem Commun.(Camb)* **2007**, (37), 3817–3819.

[8] Jacquemin, J.; Ge, R.; Nancarrow, P.; Rooney, D. W.; Costa Gomes, M. F.; Pádua, A. A. H.; Hardacre, C. *J. Chem. Eng. Data.* **2008**, *53*(3), 716–726.

[9] Schultz, A. J.; Hall, C. K.; Genzer, J. *Macromolecules* **2007**, *40*(8), 2629–2632.

[10] Walden, P. *Bull. Acad. Imper. Sci.* **1914**, page 405.

[11] Newington, I.; Juan M. Perez-Arlandis, a.; Welton, T. *Org. Lett.* **2007**, *9*(25), 5247–5250.

[12] Plechkova, N. V.; Seddon, K. R. *Methods and Reagents for Green Chemistry* **2007**, pages 105–130.

[13] Marsh, K.; Boxall, J.; Lichtenthaler, R. *Fluid Phase Equilib.* **2004**, *219*(1), 93 – 98.

[14] Earle, M. J.; Esperanca, J. M.; Gilea, M. A.; Canongia Lopes, J. N.; Rebelo, L. P.; Magee, J. W.; Seddon, K. R.; Widegren, J. A. *Nature* **2006**, *439*(7078), 831–834.

[15] Kosmulski, M.; Gustafsson, J.; Rosenholm, J. B. *Thermochim. Acta* **2004**, *412*, 47 – 53.

[16] Fox, D. M.; Gilman, J. W.; Morgan, A. B.; Shields, J. R.; Maupin, P. H.; Lyon, R. E.; Long, H. C. D.; Trulove, P. C. *Ind. Eng. Chem. Res.* **2008**, *47*(16), 6327–6332.

[17] Galiński, M.; Lewandowski, A.; Stepniak, I. *Electrochim. Acta* **2006**, *51*(26), 5567 – 5580.

[18] Rocha, M. A. A.; Neves, C. M. S. S.; Freire, M. G.; Russina, O.; Triolo, A.; Coutinho, J. A. P.; Santos, L. M. N. B. F. *J. Phys. Chem. B* **2013**, *117*(37), 10889–10897.

[19] Pádua, A. A. H.; Costa Gomes, M. F.; Canongia Lopes, J. N. A. *Acc. Chem. Res.* **2007**, *40*(11), 1087–1096.

[20] Hiroyuki, T.; Kikuko, H.; Kunikazu, I.; Md. Abu Bin, H. S.; Watanabe, M. *J. Phys. Chem. B* **2005**, *109*(13), 6103–6110.

[21] Russina, O.; Triolo, A.; Gontrani, L.; Caminiti, R. *J. Phys. Chem. Lett.* **2012**, *3*(1), 27–33.

[22] Russina, O.; Triolo, A. *Faraday Discuss.* **2012**, *154*, 97–109.

[23] Armand, M.; Endres, F.; MacFarlane, D. R.; Ohno, H.; Scrosati, B. *Nat. Mater.* **2009**, *8*(8), 621–629.

[24] Tarascon, J. M.; Armand, M. November **2001**, *414*(6861), 359–367.

[25] Alper, J. *Science* **2002**, *296*(5571), 1224–1226.

[26] Shin, J. H.; Henderson, W. A.; Passerini, S. *Electrochem. Solid-State Lett.* **2005**, *8*(2), A125–A127.

[27] MacFarlane, D. R.; Forsyth, M.; Howlett, P. C.; Kar, M.; Passerini, S.; Pringle,

J. M.; Ohno, H.; Watanabe, M.; Yan, F.; Zheng, W.; Zhang, S.; Zhang, J. *Nat. Mater.* **2016**, *1*, 15005.

[28] Simon, P.; Gogotsi, Y. *Nat. Mater.* **2008**, *7*(11), 845–854.

[29] Wasserscheid, P.; Welton, T. *Ionic liquids in synthesis*, Vol. 1; Wiley Online Library, 2008.

[30] Chowdhury, S.; Mohan, R. S.; Scott, J. L. *Tetrahedron* **2007**, *63*(11), 2363 – 2389.

[31] Zhao, H. *J. Mol. Catal. B: Enzym.* **2005**, *37*(16), 16 – 25.

[32] van Rantwijk, F.; Sheldon, R. A. *Chem. Rev.* **2007**, *107*(6), 2757–2785.

[33] Matsuda, T. *Future directions in biocatalysis;* Elsevier, 2011.

[34] Lozano, P. *Green Chem.* **2010**, *12*, 555–569.

[35] Wei, G.; Yang, Z.; Chen, C. *Anal. Chim. Acta* **2003**, *488*(2), 183 – 192.

[36] Visser, A. E.; Swatloski, R. P.; Reichert, W. M.; Mayton, R.; Sheff, S.; Wierzbicki, A.; Davis Jr, J. H.; Rogers, R. D. *Chem. Commun.* **2001**, pages 135–136.

[37] Germani, R.; Mancini, M. V.; Savelli, G.; Spreti, N. *Tetrahedron Lett.* **2007**, *48*(10), 1767 – 1769.

[38] Bates, E. D.; Mayton, R. D.; Ntai, I.; Davis, J. H. *J. Am. Chem. Soc.* **2002**, *124*(6), 926–927.

[39] Moniruzzaman, M.; Tamura, M.; Tahara, Y.; Kamiya, N.; Goto, M. *Int. J. Pharm.* **2010**, *400*, 243 – 250.

[40] Mizuuchi, H.; Jaitely, V.; Murdan, S.; Florence, A. *Eur. J. Pharm. Sci.* **2008**, *33*(45), 326 – 331.

[41] Allen, M. P.; Tildesley, D. J. *Computer simulation of liquids;* Oxford university press, 1989.

[42] Gromacs user manual version 4.5.6. van der Spoel, D.; Lindahl, E.; Hess, B.; van Buuren, A. R.; Apol, E.; Meulenhoff, P. J.; Tieleman, D. P.; Sijbers, A. L. T. M.; Feenstra, K. A.; van Drunen, R.; Berendsen, H. J. C.; GROMACS development team, **2013**.

[43] Hansson, T.; Oostenbrink, C.; van Gunsteren, W. *Current Opinion in Structural Biology* **2002**, *12*(2), 190 – 196.

[44] Andersen, H. C. *J. Chem. Phys.* **1980**, *72*(4), 2384–2393.

[45] Kukol, A. *Molecular modeling of proteins;* Springer, second ed., 2008.

[46] Andrew, R. L. *Molecular modelling: principles and applications;* Prentice Hall, 2001.

[47] Rizzo, R. C.; Jorgensen, W. L. *J. Am. Chem Soc.* **1999**, *121*(20), 4827–4836.

[48] Price, M. L. P.; Ostrovsky, D.; Jorgensen, W. L. *J. Comput. Chem.* **2001**, *22*(13), 1340–1352.

[49] Jorgensen, W. L.; Maxwell, D. S.; Tirado-Rives, J. *J. Am. Chem. Soc.* **1996**, *118*(45), 11225–11236.

[50] Hahn, T.; Shmueli, U.; Wilson, A. A. J. C.; Prince, E. *International tables for crystallography;* D. Reidel Publishing Company, 2005.

[51] Lorch, E. *J. Phys. C: Solid State Phys.* **1969**, *2*, 229–237.

[52] Du, J.; Benmore, C. J.; Corrales, R.; Hart, R. T.; Weber, J. K. R. *J. Phys.: Condens. Matter* **2009**, *21*(20), 205102.

[53] Santos, C. S.; Annapureddy, H. V. R.; Murthy, N. S.; Kashyap, H. K.; Castner, Jr., E. W.; Margulis, C. J. *J. Chem. Phys.* **2011**, *134*(6), 064501.

[54] Kashyap, H. K.; Santos, C. S.; Annapureddy, H. V. R.; Murthy, N. S.; Margulis, C. J.; Castner, Jr., E. W. *Faraday Discuss.* **2012**, *154*, 133–143.

[55] Kashyap, H. K.; Margulis, C. J. *ECS Trans.* **2013**, *50*, 301–307.

[56] Kashyap, H. K.; Hettige, J. J.; Annapureddy, H. V. R.; Margulis, C. J. *Chem. Commun.* **2012**, *48*, 5103–5105.

[57] Hansen, J.; McDonald, I. *Theory of Simple Liquids;* Elsevier Science, third ed., 2006.

[58] Van Der Spoel, D.; Lindahl, E.; Hess, B.; Groenhof, G.; Mark, A. E.; Berendsen, H. J. C. *J. Comput. Chem.* **2005**, *26*(16), 1701–1718.

[59] Hess, B.; Kutzner, C.; Van Der Spoel, D.; Lindahl, E. *J. Chem. Theory Comput.* **2008**, *4*(3), 435–447.

[60] Nosé, S. *Mol. Phys.* **1984**, *52*, 255 – 268.

[61] Nosé, S. *J. Chem. Phys.* **1984**, *81*, 511–519.

[62] Parrinello, M.; Rahman, A. *J. Appl. Phys.* **1981**, *52*(12), 7182–7190.

[63] Essmann, U.; Perera, L.; Berkowitz, M. L.; Darden, T.; Lee, H.; Pedersen, L. G. *J. Chem. Phys.* **1995**, *103*(19), 8577–8593.

[64] Darden, T.; York, D.; Pedersen, L. *J. Chem. Phys.* **1993**, *98*(12), 10089–10092.

[65] P. C. Howlett, E. I. Izgorodina, M. F.; MacFarlane, D. R. *Z. Phys. Chem.* **2006**, *220*, 1483–1498.

[66] Henderson, W. A.; Young, V. G.; Pearson, W.; Passerini, S.; De Long, H. C.; Trulove, P. C. *J. Phys.: Condens. Matter* **2006**, *18*(46), 10377–10390.

[67] Li, S.; Banuelos, J. L.; Guo, J.; Anovitz, L.; Rother, G.; Shaw, R. W.;

Hillesheim, P. C.; Dai, S.; Baker, G. A.; Cummings, P. T. *J. Phys. Chem. Lett.* **2012**, *3*(1), 125–130.

[68] Lopes, J. N. C.; Pádua, A. A. H. *J. Phys. Chem. B* **2004**, *108*(43), 16893–16898.

[69] Canongia Lopes, J. N.; Pádua, A. A. H. *J. Phys. Chem. B* **2004**, *108*(43), 16893–16898.

[70] Urahata, S. M.; Ribeiro, M. C. C. *J. Chem. Phys.* **2004**, *120*(4), 1855–1863.

[71] Del Popolo, M. G.; Voth, G. A. *J. Phys. Chem. B* **2004**, *108*, 1744–1752.

[72] Wang, Y.; Voth, G. A. *J. Am. Chem. Soc.* **2005**, *127*(35), 12192–12193.

[73] Wang, Y. T.; Izvekov, S.; Yan, T. Y.; Voth, G. A. *J. Phys. Chem. B* **2006**, *110*(8), 3564–3575.

[74] Borodin, O.; Smith, G. D. June **2006**, *110*(23), 11481–11490.

[75] Bhargava, B. L.; Devane, R.; Klein, M. L.; Balasubramanian, S. *Soft Matter* **2007**, *3*, 1395–1400.

[76] Lopes, J. N. C.; Pádua, A. A. H. *J. Phys. Chem. B* **2006**, *110*, 3330–3335.

[77] Canongia Lopes, J. N.; Shimizu, K.; Pádua, A. A. H.; Umebayashi, Y.; Fukuda, S.; Fujii, K.; Ishiguro, S. *J. Phys. Chem. B* **2008**, *112*(5), 1465–1472.

[78] Kashyap, H. K.; Santos, C. S.; Annapureddy, H. V. R.; Murthy, N. S.; Margulis, C. J.; Castner, Jr., E. W. *Faraday Discuss.* **2012**, *154*, 133–143.

[79] Triolo, A.; Russina, O.; Caminiti, R.; Shirota, H.; Lee, H. Y.; Santos, C. S.; Murthy, N. S.; Castner, Jr, E. W. *Chem. Commun.* **2012**, *48*, 4959–4961.

[80] Gontrani, L.; Russina, O.; Celso, F. L.; Caminiti, R.; Annat, G.; Triolo, A. *J. Phys. Chem. B* **2009**, *113*(27), 9235–9240.

[81] Russina, O.; Lo Celso, F.; Di Michiel, M.; Passerini, S.; Appetecchi, G. B.; Castiglione, F.; Mele, A.; Caminiti, R.; Triolo, A. *Faraday Discuss.* **2013**, *167*, 499–513.

[82] Russina, O.; Triolo, A. *Faraday Discuss.* **2012**, *154*(0), 97–109.

[83] Bodo, E.; Gontrani, L.; Caminiti, R.; Plechkova, N. V.; Seddon, K. R.; Triolo, A. *J. Phys. Chem. B* **2010**, *114*(49), 16398–16407.

[84] Zheng, W.; Mohammed, A.; Hines, L. G.; Xiao, D.; Martinez, O. J.; Bartsch, R. A.; Simon, S. L.; Russina, O.; Triolo, A.; Quitevis, E. L. *J. Phys. Chem. B* **2011**, *115*(20), 6572–6584.

[85] Li, S.; Bañuelos, J. L.; Guo, J.; Anovitz, L.; Rother, G.; Shaw, R. W.; Hillesheim, P. C.; Dai, S.; Baker, G. A.; Cummings, P. T. *J. Phys. Chem. Lett.* **2012**, *3*(1), 125–130.

[86] Canongia Lopes, J. N.; Pádua, A. A. *J. Phys. Chem. B* **2006**, *110*(39), 19586.

[87] Canongia Lopes, J. N.; Deschamps, J.; Padua, A. A. H. *J. Phys. Chem. B* **2004**, *108*(6), 2038–2047.

[88] Nakayama, H.; Kuwata, H.; Yamamoto, N.; Akagi, Y.; Matsui, H. *Bull. Chem. Soc. Jpn.* **1989**, *62*(4), 985–992.

[89] Lind Jr, J. E.; Abdel-Rehim, H.; Rudich, S. *J. Phys. Chem.* **1966**, *70*(11), 3610–3619.

[90] Scurto, A. M.; Newton, E.; Weikel, R. R.; Draucker, L.; Hallett, J.; Liotta, C. L.; Leitner, W.; Eckert, C. A. *Ind. Eng. Chem. Res.* **2008**, *47*(3), 493–501.

[91] Matsumoto, H.; Kageyama, H.; Miyazaki, Y. *Chem. Lett.* **2001**, (2), 182–183.

[92] MacFarlane, D.; Forsyth, S.; Golding, J.; Deacon, G. *Green Chem.* **2002**, *4*(5), 444–448.

[93] Li, S.; Feng, G.; Bañuelos, J. L.; Rother, G.; Fulvio, P. F.; Dai, S.; Cummings, P. T. *J. Phys. Chem. C* **2013**, *117*(35), 18251–18257.

[94] Canongia Lopes, J. N. A.; Pádua, A. A. H. *J. Phys. Chem. B* **2006**, *110*(7), 3330–3335.

[95] Russina, O.; Gontrani, L.; Fazio, B.; Lombardo, D.; Triolo, A.; Caminiti, R. *Chem. Phys. Lett.* **2010**, *493*(4), 259 – 262.

[96] Triolo, A.; Mandanici, A.; Russina, O.; Rodriguez-Mora, V.; Cutroni, M.; Hardacre, C.; Nieuwenhuyzen, M.; Bleif, H.; Keller, L.; Ramos, M. A. *J. Phys. Chem. B* **2006**, *110*(42), 21357–21364.

[97] Triolo, A.; Russina, O.; Bleif, H.; Di Cola, E. *J. Phys. Chem. B* **2007**, *111*(18), 4641–4644.

[98] Nemoto, F.; Kofu, M.; Yamamuro, O. *J. Phys. Chem. B* **2015**, *119*(15), 5028–5034.

[99] Hettige, J. J.; Kashyap, H. K.; Annapureddy, H. V. R.; Margulis, C. J. *J. Phys. Chem. Lett.* **2013**, *4*(1), 105–110.

[100] Kashyap, H. K.; Santos, C. S.; Murthy, N. S.; Hettige, J. J.; Kerr, K.; Ramati, S.; Gwon, J.; Gohdo, M.; Lall-Ramnarine, S. I.; Wishart, J. F.; Margulis, C. J.; Castner, Jr., E. W. *J. Phys. Chem. B* **2013**, *117*(49), 15328–15337.

[101] Kashyap, H. K.; Santos, C. S.; Daly, R. P.; Hettige, J. J.; Murthy, N. S.; Shirota, H.; Castner, Jr., E. W.; Margulis, C. J. *J. Phys. Chem. B* **2013**, *117*(4), 1130–1135.

[102] Araque, J. C.; Hettige, J. J.; Margulis, C. J. *J. Phys. Chem. B* **2015**, *119*(40), 12727–12740.

[103] Liu, X.; Zhou, G.; Zhang, S.; Yu, G. *Mol. Simul.* **2010**, *36*, 79–86.

[104] Liang, M.; Khatun, S.; Castner, E. W. *J. Chem. Phys.* **2015**, *142*(12).

[105] Blesic, M.; Lopes, J. N. C.; Gomes, M. F. C.; Rebelo, L. P. N. *Phys. Chem. Chem. Phys.* **2010**, *12*, 9685–9692.

[106] Gupta, A.; Sharma, S.; Kashyap, H. K. *J. Chem. Phys.* **2015**, *142*(13), 134503.

[107] Hettige, J. J.; Kashyap, H. K.; Margulis, C. J. *J. Chem. Phys.* **2014**, *140*(11), 111102.

[108] Canongia Lopes, J. N.; Pádua, A. A., A. A. H.; Shimizu, K. *J. Phys. Chem. B* **2008**, *112*(16), 5039–5046.

[109] Canongia Lopes, J. N. A.; Padua, A. A. H. *J. Phys. Chem. B* **2006**, *110*(7), 3330–3335.

[110] Araque, J. C.; Yadav, S. K.; Shadeck, M.; Maroncelli, M.; Margulis, C. J. *J. Phys. Chem. B* **2015**, *119*, 70157029.

[111] Griffin, P. J.; Holt, A. P.; Tsunashima, K.; Sangoro, J. R.; Kremer, F.; Sokolov, A. P. *J. Chem. Phys.* **2015**, *142*(8).

[112] Shirota, H.; Fukazawa, H.; Fujisawa, T.; Wishart, J. F. *J. Phys. Chem. B* **2010**, *114*(29), 9400–9412.

[113] Sesto, R. E. D.; Corley, C.; Robertson, A.; Wilkes, J. S. *J. Organomet. Chem.* **2005**, *690*(10), 2536 – 2542.

[114] McAtee, Z. P.; Heitz, M. P. *J. Chem. Thermodyn.* **2016**, *93*, 34 – 44.

[115] Neves, C. M.; Carvalho, P. J.; Freire, M. G.; Coutinho, J. A. *J. Chem. Thermodyn.* **2011**, *43*(6), 948 – 957.

[116] Steinhardt, P. J.; Nelson, D. R.; Ronchetti, M. *Physical Review B* **1983**, *28*(2), 784.

[117] Shimizu, K.; Bernardes, C. E. S.; Triolo, A.; Canongia Lopes, J. N. *Phys. Chem. Chem. Phys.* **2013**, *15*, 16256–16262.

[118] Freitas, A. A.; Shimizu, K.; Canongia Lopes, J. N. *J. Chem. Eng. Data* **2014**, *59*(0), 3120–3129.

[119] Yoshida, Y.; Saito, G. *Phys. Chem. Chem. Phys.* **2011**, *13*(45), 20302.

[120] Pereiro, A. B.; Pastoriza-Gallego, M. J.; Shimizu, K.; Marrucho, I. M.; Lopes, J. N. C.; Piñeiro, M. M.; Rebelo, L. P. N. *J. Phys. Chem. B* **2013**, *117*(37), 10826–10833.

[121] Shen, Y.; Kennedy, D. F.; Greaves, T. L.; Weerawardena, A.; Mulder, R. J.; Kirby, N.; Song, G.; Drummond, C. J. *Phys. Chem. Chem. Phys.* **2012**, *14*, 7981–7992.

[122] Hayes, R.; Imberti, S.; Warr, G. G.; Atkin, R. *J. Phys. Chem. C* **2014**, *118*(25), 13998–14008.

[123] Hayes, R.; Imberti, S.; Warr, G. G.; Atkin, R. *Angewandte Chemie* **2013**, *125*(17), 4721–4725.

[124] Hayes, R.; Imberti, S.; Warr, G. G.; Atkin, R. *Phys. Chem. Chem. Phys.* **2011**, *13*, 3237–3247.

[125] Hayes, R.; Imberti, S.; Warr, G. G.; Atkin, R. *Phys. Chem. Chem. Phys.* **2011**, *13*, 13544–13551.

[126] Atkin, R.; Warr, G. G. *J. Phys. Chem. B* **2008**, *112*(14), 4164–4166.

[127] Turton, D. A.; Sonnleitner, T.; Ortner, A.; Walther, M.; Hefter, G.; Seddon, K. R.; Stana, S.; Plechkova, N. V.; Buchner, R.; Wynne, K. *Faraday Discuss.* **2012**, *154*, 145–153.

[128] Ishiguro, S.; Umebayashi, Y.; Kanzaki, R.; Fujii, K. *Pure Appl. Chem.* **2010**, *82*(10), 1927–1941.